ACCSCIENCE PUBLISHING

Materials Science in Additive Manufacturing

REVIEW ARTICLE

# Laser additive manufacturing of nickel-based superalloys: A review

**Yunlong Hu[1]*, Zihong Wang[1]*, Qiang Zhang[1], Shan Li[1], Xin Zhang[2], and Weidong Huang[2]**

[1]Department of Structural Materials Research, Suzhou Laboratory, Suzhou, Jiangsu, China

[2]State Key Laboratory of Solidification Processing, Northwestern Polytechnical University, Xi'an, Shaanxi, China

(This article belongs to the *Special Issue*: *Additive Manufacturing of Materials for Extreme Environments*)

## Abstract

Nickel-based superalloys are critical materials for high-temperature components in core equipment, such as aerospace engines and gas turbines. In recent years, with the rapid advancement of metal additive manufacturing (AM) technologies, the fabrication of complex geometries using nickel-based superalloys has been successfully applied in modern engines and gas turbines. These components demonstrate significant advantages in integration, weight reduction, multifunctionality, and performance enhancement. However, due to the complex alloy composition and multiphase microstructure of nickel-based superalloys, the AM process is accompanied by intricate phase transformations and high thermal stresses. This often leads to defects, such as hot cracking—particularly in the vicinity of the molten pool. In addition, the rapid non-equilibrium solidification and repeated thermal cycles from layer-by-layer deposition result in complex microstructural evolution and phase transformations during both solidification and subsequent solid-state reactions. These factors significantly influence the strengthening and toughening behavior of the superalloys. Consequently, the comprehensive mechanical properties of additively manufactured nickel-based superalloys still lag behind those of their traditionally forged counterparts. This article reviews recent domestic and international research progress on the mechanisms of crack formation and control strategies in AM of nickel-based superalloys, as well as the evolution of microstructure and the associated strengthening and toughening mechanisms. Furthermore, it discusses the design of nickel-based superalloys tailored specifically for AM, and offers insights and future perspectives on the development of advanced strengthening strategies and alloy design methodologies for AM applications.

***Keywords:*** Additive manufacturing; Nickel-based superalloy; Cracking mechanism; Microstructural evolution; Strengthening mechanism; Alloy design

***Corresponding authors:**
Yunlong Hu
(huyl@szlab.ac.cn)
Zihong Wang
(wangzh@szlab.ac.cn)

**Citation:** Hu Y, Wang Z, Zhang Q, Li S, Zhang X, Huang W. Laser additive manufacturing of nickel-based superalloys: A review. *Mater Sci Add Manuf*. 2026;5(1):025240051. doi: 10.36922/MSAM025240051

**Received:** June 14, 2025

**Revised:** August 07, 2025

**Accepted:** August 11, 2025

**Published online:** October 31, 2025



## 1. Introduction

High-temperature alloys refer to materials capable of maintaining long-term structural stability and operational performance at temperatures above 600°C. They exhibit excellent mechanical properties at both room and elevated temperatures, including high

static mechanical strength, creep resistance at elevated temperatures, and fatigue performance. In addition, they possess good oxidation and corrosion resistance, as well as exceptional microstructural stability under harsh service conditions. As a result, they are extensively employed in aerospace engines, gas turbines, and petrochemical industries.[1] Based on their matrix composition, high-temperature alloys can be classified into iron-based, nickel-based, and cobalt-based alloys. Compared to iron-based and cobalt-based superalloys, nickel-based superalloys feature a single-phase crystal structure (face-centered cubic [FCC] structure) and do not undergo allotropic transformations at high temperatures, which enhance their structural stability. Moreover, the nickel matrix can dissolve a large quantity of strengthening elements, such as aluminum, molybdenum, niobium, tungsten, and titanium, allowing for a high degree of alloying and the formation of multiple strengthening phases within the matrix. Consequently, nickel-based superalloys demonstrate superior mechanical performance. In addition, nickel has a high melting point and excellent chemical stability, which endows these alloys with remarkable oxidation and corrosion resistance. For these reasons, nickel-based superalloys are the most widely used and extensively developed class of high-temperature alloys.[2]

In recent years, with the rapid advancement of technologies in modern aero-engines and gas turbines, increasingly stringent requirements have been placed on the structure, performance, and functionality of their hot-section components. The integrated structural and functional design of complex components in aero-engines and gas turbines can significantly improve lightweight characteristics, functional performance, and mechanical properties, and has gradually become a key direction in the design and manufacturing of high-performance complex components in this field. However, currently, 30–45% of hot-section components in aero-engines and gas turbines are manufactured from high-temperature alloys using forging processes, followed by subtractive machining, which often results in substantial material waste. Moreover, high-temperature alloys generally exhibit poor formability and machinability, making the production of complex structural components even more challenging. As a result, in actual component design and manufacturing processes, design compromises are frequently made regarding functionality and lightweight features due to limitations in current machining technologies,[2,3] which severely restrict innovation and development in aero-engine and gas turbine technologies.

Metal additive manufacturing (AM), also known as 3D printing, is an advanced, freeform digital manufacturing method that has created a transformative pathway for the integrated structural-functional manufacturing of complex components in aero-engines and gas turbines. Meanwhile, it can also strengthen metallic materials, thereby improving their mechanical properties. At present, the mainstream high-performance laser AM (LAM) technologies for metals are primarily categorized into two types: laser-directed energy deposition (LDED) and laser powder bed fusion (LPBF). LDED enables efficient fabrication of complex, high-performance components, with virtually no size limitation of the final part. Moreover, LDED features *in situ* material feeding (using metal powders or wires), which allows for arbitrary multi-material integration and the creation of functionally graded structures within a single component, providing a technological foundation for multifunctional design. In contrast, although LPBF has relatively lower build efficiency, it offers superior dimensional accuracy and surface finish, making it particularly suitable for producing intricate and highly detailed geometries.[3-7] With the rapid development of AM technologies, numerous companies have successfully implemented metal AM in the production of critical high-performance components for aero-engines and gas turbines. It has been demonstrated that metal AM can: (i) achieve near-net shaping of complex components with significantly improved material utilization; (ii) enhance lightweight design and overall performance; and (iii) shorten research and production cycles, thereby reducing manufacturing costs. For example, General Electric (GE) in the United States (U.S.) optimized the design of the fuel nozzle for the LEAP-1A engine and utilized AM to fabricate a previously unachievable complex internal channel structure using conventional manufacturing methods.[7,8] This innovation enabled the integration of over 20 individual components into a single, monolithic part, which was manufactured in a single process step. As a result, fuel efficiency and nozzle durability were significantly improved. The redesigned nozzle is expected to reduce fuel consumption and emissions of the LEAP engine by approximately 15%. At present, LEAP engines equipped with additively manufactured fuel nozzles have been installed on the Airbus A320neo aircraft, with the first successful flight completed on May 19, 2015. The engine has been certified by both the European Aviation Safety Agency and the U.S. Federal Aviation Administration. At the 2017 Paris Air Show, GE announced that LEAP engines containing additively manufactured components had generated $31 billion in orders for the company.[9]

At present, the number of nickel-based superalloy components fabricated through AM for commercial applications remains relatively limited, and the range of nickel-based superalloys suitable for AM is also quite

narrow. This limitation primarily stems from the complex alloy composition and phase structure of nickel-based superalloys, as well as the intricate metallurgical behaviors and high thermal stresses that occur during the AM process, making them highly susceptible to defects such as hot cracking. The near-rapid, non-equilibrium solidification within the melt pool, coupled with repeated thermal cycling and associated solid-state phase transformations, further complicates microstructural evolution. Moreover, the diverse strengthening and toughening mechanisms inherent to nickel-based superalloys introduce additional challenges in achieving consistent control over mechanical properties. Although the mechanical performance of additively manufactured nickel-based superalloys has, in some cases, exceeded that of their forged counterparts, the available data often exhibit significant variability, with notable differences observed between different batches. As a result, research on the AM of nickel-based superalloys remains predominantly at the laboratory scale, hindering their widespread adoption in commercial applications.[10]

In addition, most of the nickel-based superalloys currently studied for AM are conventional commercial alloys, including cast superalloys (such as K465, IN738, DZ125, and CM247LC), wrought superalloys (such as Inconel 718, Inconel 625, and Hastelloy X [HX]), and powder metallurgy superalloys (such as IN100, Rene95, Rene88DT, and FGH4096). A review of the development history of superalloys reveals that alloy composition is closely tied to the processing method. To enhance mechanical properties, cast nickel-based superalloys typically contain relatively high levels of aluminum and titanium, resulting in a higher volume fraction of strengthening phases. However, this also makes them prone to macro- and micro-segregation during solidification, as well as the formation of coarse eutectic phases at the end of solidification, which negatively affects their weldability. In single-crystal superalloys, to avoid the formation of stray grains and low-angle grain boundaries, the content of grain boundary strengthening elements, such as carbon, boron, zirconium, and magnesium, is typically kept very low or even eliminated. In wrought superalloys, to reduce deformation resistance during plastic forming and to prevent cracking during forging, the aluminum and titanium contents are relatively low, and the volume fraction of strengthening phases is generally below 40%, which limits the extent of performance improvement achievable. In contrast, powder metallurgy superalloys completely avoid the solidification process, thereby minimizing elemental segregation. These alloys typically exhibit a higher volume fraction of strengthening phases (usually above 45%), leading to superior mechanical properties compared to wrought superalloys. This analysis highlights that the composition design of nickel-based superalloys has traditionally been optimized to align with the specific characteristics of their respective manufacturing processes. Since the processing characteristics of AM differ significantly from those of conventional methods, traditional commercial nickel-based superalloys may not be well-suited. Therefore, it is essential to develop novel nickel-based superalloys specifically tailored for AM to meet its unique requirements and promote the industrial application of additively manufactured nickel-based superalloys.[10]

The present review focuses on nickel-based superalloys, which are widely used as high-temperature structural materials for hot-section components in aerospace engines and gas turbines. It provides a comprehensive assessment of recent research progress, both domestically and internationally, in cracking mechanisms and crack prevention strategies in additively manufactured nickel-based superalloys, microstructural evolution, and underlying strengthening-toughening mechanisms, as well as alloy composition design specifically tailored for AM. Furthermore, this review presents insights and forward-looking perspectives on the future development of additively manufactured nickel-based superalloys.

## 2. Cracking mechanisms and crack control in additively manufactured nickel-based superalloys

Cracking is a prevalent issue in additively manufactured nickel-based superalloys. It has been observed not only in cast superalloys with poor weldability (such as K465,[11,12] DZ125,[13,14] CM247LC,[15,16] and IN738[17,18]) but also in powder metallurgy superalloys with good weldability (such as Rene 104,[19,20] Rene 88DT,[21,22] and IN100[23]), and even in wrought superalloys with relatively low crack sensitivity (such as Inconel 718[24-27], Inconel 625[28-30], and HX[31-37]). The presence of cracks significantly degrades the mechanical properties of the material, rendering it unsuitable for service applications. Therefore, understanding the cracking mechanisms and developing effective crack control strategies are critical priorities in the AM of nickel-based superalloys.

The metallurgical processes occurring in the melt pool during AM are comparable to those in welding. Therefore, established principles from welding metallurgy can be referenced to investigate the cracking mechanisms in additively manufactured nickel-based superalloys. According to well-established knowledge in the welding metallurgy of nickel-based superalloys, hot cracking is a prevalent metallurgical defect, and the primary types of cracks include solidification cracking (SC), liquation

cracking (LC), ductility dip cracking (DDC), and strain-age cracking (SAC).[38] SC occurs during the final stage of solidification when a low-melting-point eutectic liquid film forms between dendrites. Under the influence of shrinkage and thermal stresses, this film ruptures. Due to the closure of feeding channels, insufficient compensation for shrinkage leads to crack formation, typically located between dendrites and along grain boundaries. The key metallurgical factors influencing the SC susceptibility of nickel-based superalloys include the solidification temperature range, the amount and distribution of interdendritic liquid during late-stage solidification, and the morphology and size of grains. In general, the larger the solidification temperature range, the higher the susceptibility to SC.[39]

LC occurs in the heat-affected zone (HAZ) near the deposited layer during AM, where the material remains within the temperature range between the solidus and liquidus for an extended period. Within this range, some low-melting-point eutectic phases may partially remelt, forming liquid films that cannot withstand the applied stress, leading to crack initiation—most commonly along grain boundaries. DDC typically occurs in pure metals or single-phase austenitic alloys. Within the temperature range of $0.5T_S$ to $T_S$ (where $T_S$ is the solidus temperature), the material's ductility experiences a sharp decline. When localized deformation exceeds the critical strain limit under stress, cracks may form. As this type of cracking occurs in the solid state, it is also referred to as solid-state cracking. DDC is closely associated with grain boundary migration and is frequently observed at grain boundaries. SAC develops during reheating or subsequent heat treatment and is specific to precipitation-strengthened nickel-based superalloys. When the temperature range for precipitate formation overlaps with the stress relaxation range during heating, high local stresses can develop at grain boundaries. If the local stress exceeds a critical threshold, grain boundary failure occurs, resulting in SAC. The volume fraction of precipitates is the main factor affecting SAC susceptibility; the higher the aluminum and titanium content, the greater the cracking susceptibility.[40] The main types of cracking and their characteristics in additively manufactured nickel-based superalloys are displayed in Figure 1.

The AM process of nickel-based superalloys involves rapid cooling of small melt pools and repeated thermal cycling of the fabricated part, which leads to the development of significant thermal and residual stresses.[43-46] Although the near-rapid solidification in the melt pool during AM can effectively prevent macroscopic segregation, microscopic segregation still occurs—and in some cases, it may be even more severe than that observed in conventional casting. During solidification, alloying elements with equilibrium partition coefficients <1 tend to segregate into the interdendritic regions. This microsegregation results in a wider solidification temperature range and facilitates the formation of low-melting-point eutectic liquid phases between dendrites in nickel-based superalloys,[47-51] thereby promoting liquid film formation and further increasing susceptibility to SC and LC. Furthermore, repeated thermal cycling can expose already-deposited material to elevated temperatures that fall within the brittle temperature range of the alloy. At such temperatures, the alloy exhibits reduced ductility, making it more susceptible to DDC under thermal stress. In the case of precipitation-strengthened nickel-based superalloys, precipitate phases may form during thermal cycling, increasing the risk of SAC. Ojo *et al.*,[52,53] in their study of the welding of IN-738 alloy, observed that cracks primarily formed at grain boundaries within the HAZ, a characteristic feature of LC. They attributed this phenomenon to the rapid heating during welding, which prevented the complete dissolution of coarse γ' particles located at grain boundaries. The residual γ' then underwent a eutectic reaction with the surrounding γ matrix ($\gamma + \gamma' \rightarrow L$), resulting in the formation of a liquid film. In addition, grain-boundary M(Ti, Mo, W)C (MC) carbides, borides, and carbon-sulfide inclusions were found to experience similar liquation reactions, further promoting liquid film formation and crack initiation under stress. Other researchers have proposed that the liquid film in the HAZ may also arise from the direct melting of low-melting-point eutectic phases at grain boundaries.[54] Xu *et al.*,[41] in a study on laser solid-formed IN738LC superalloys, found that liquation cracks in the HAZ were predominantly located along grain boundaries. The primary cause of this liquation was the melting of low-melting γ–γ' eutectic at grain boundaries during processing, leading to continuous or semi-continuous liquid films. Moreover, boron enrichment at grain boundaries was found to lower the local melting temperature. It was, further, clarified that the liquation observed in laser solid-formed IN738LC was primarily due to direct eutectic melting rather than compositional liquation. This observation was supported by the fine size (~100 nm) and coherent nature of the γ' particles with the γ matrix, which implied that their dissolution was interface-controlled, resulting in a slow increase in solute concentration at the γ/γ' interface and thereby suppressing compositional liquation during rapid heating. In multilayer, multipass specimens, the overlapping regions exhibited the most severe cracking, with both liquation and solidification cracks present. Solidification cracks in the melt pool of the

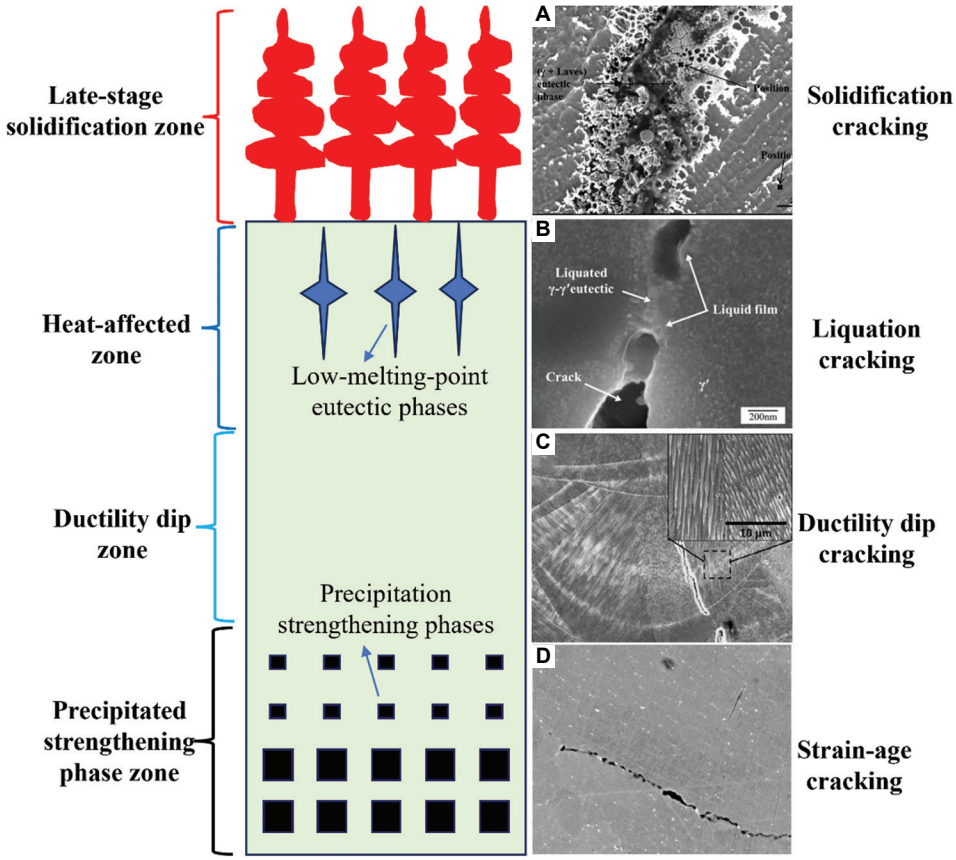


**Figure 1.** Cracking types and the characteristics of additively manufactured nickel-based superalloys. (A) Solidification cracking. Adapted with permission from Hu *et al.*[39] Copyright © 2017 Elsevier Ltd. (B) Liquation cracking. Adapted with permission from Xu *et al.*[41] Copyright © 2018 Elsevier Ltd. (C) Ductility dip cracking. Adapted with permission from Cloots *et al.*[42] Copyright © 2016 Elsevier Ltd. (D) Strain-age cracking. Adapted with permission from Li *et al.*[14] Copyright © 2018 Elsevier Ltd

overlay layer were observed to propagate directly from pre-existing liquation cracks in the HAZ. This crack linkage was attributed to a mismatch in thermal flow direction on either side of the overlap region, promoting the formation of high-angle grain boundaries. These boundaries have a lower complete solidification temperature and higher wettability compared to low-angle grain boundaries, making them more susceptible to liquid film spreading and, consequently, to crack initiation and propagation. Residual stress analysis of these specimens revealed that stress in the overlap zones was 300 MPa higher than in the bead interiors, providing a strong driving force for crack formation.

In the laser solid-forming process of Inconel 625, the present authors observed the segregation of alloying elements, such as Nb and Mo, into the interdendritic regions during solidification. This promoted the formation of Laves phases, which increased the alloy's solidification temperature range from 90°C to 210°C and significantly raised its susceptibility to SC.[39] In addition, the high thermal gradients inherent in the laser-forming process induced large thermal stresses in the deposited layers. These stresses acted on the thin, continuous liquid films present between dendrites at the end of solidification, leading to crack initiation. The mushy zone in Inconel 625 was found to be relatively wide, yet with a low liquid phase volume fraction. As a result, feeding channels became blocked, and the liquid phase could not adequately compensate for solidification shrinkage, allowing cracks to persist in the deposited layers. Chen *et al.*,[55] in their investigation of the cracking mechanisms in laser-additively manufactured Inconel 718, observed both solidification and liquation cracks in as-deposited specimens. However, he emphasized that liquation cracks had a more detrimental effect on mechanical properties. Hot cracks mainly propagated along Laves phases near grain boundaries, attributed to significant elemental segregation at grain boundaries, which promoted the formation of additional low-melting-point eutectics. This segregation enhanced constitutional supercooling, lowered the local solidification temperature,

and widened the solidification temperature range—factors that collectively contributed to increased stress concentration and greater susceptibility to liquation or partially liquated hot cracking. Cloots *et al.*,[42] in their study of selective laser melting (SLM)-formed IN738LC, employed focused ion beam slicing and atom-probe tomography to perform 3D reconstructions around cracks and found that Zr segregation was a primary cause of SC. Simulation results indicated a solidification temperature of 670°C for IN738LC, with pronounced Zr enrichment in the residual liquid phase, increasing crack susceptibility. Harrison *et al.*[56] concluded that cracks in SLM-formed HX were predominantly of solid-state origin, specifically ductility dip cracks. Similarly, Zhong *et al.*[57] reported multiple cracking modes in laser-cladded IN-738, including not only LC but also non-liquation DDC and SC. SAC commonly occurs in precipitation-strengthened superalloys, with γ' phase-strengthened superalloys exhibiting higher sensitivity. There is a positive correlation between SAC sensitivity and both the volume fraction and precipitation kinetics of the strengthening precipitates.

From the above studies, it can be seen that cracking in additively manufactured nickel-based superalloys is highly complex, often involving the coexistence of two or more crack types. To address this complexity, researchers have conducted extensive studies on crack control from multiple perspectives, including process parameter optimization, substrate pre-treatment, and alloy composition modification. A common strategy involves optimizing process parameters to suppress crack formation by adjusting heat input, modifying the solidification behavior of the melt pool, or tailoring the thermal history during deposition. Such adjustments help control the size and distribution of phases and mitigate thermal stresses generated during the build process. Zhao *et al.*[58] found that adjusting the overlap ratio between adjacent deposition tracks can effectively suppress crack formation in laser solid-formed Rene88DT superalloy. When the overlap ratio is too small, a "V"-shaped depression forms between tracks, where the fraction of low-melting (γ + γ') eutectic phases is relatively high and stress concentration is more pronounced, increasing the likelihood of crack initiation. Conversely, an excessive overlap ratio leads to sloped surfaces on the deposited layers, compromising dimensional accuracy. The study identified an optimal overlap ratio of 40%, which effectively avoids both cracking and surface distortion. Furthermore, post-process hot isostatic pressing (HIP) of the as-deposited components has been demonstrated to heal small internal cracks, thereby improving structural integrity. Chen *et al.*[55] found that optimizing processing parameters during LAM of Inconel 718—specifically, using lower scan speeds and laser power—effectively reduced cracking. Moreover, a clockwise rotation of the laser beam along the scanning direction was observed to further suppress crack formation. This was attributed to the concentration of more laser energy at the front of the melt pool, which enhanced lateral heat dissipation. As a result, secondary dendrite arm growth was promoted, leading to a regular, interlocking banded microstructure that inhibited the formation of continuous, low-melting Laves phases and improved interdendritic connectivity, thereby enhancing crack resistance. In addition, this approach reduced the size of the HAZ, helping to suppress thermal cracking. In a follow-up study, carbon nanotubes (CNTs) were incorporated into Inconel 718 to evaluate their effectiveness in crack suppression. The results demonstrated that CNT addition significantly reduced cracking. This was attributed to an increased elastic modulus of the alloy, which lowered overall strain. CNTs also facilitated thermal stress transfer between dendrites, alleviating local stress concentration. Furthermore, the CNTs themselves absorbed part of the applied stress, increasing resistance to crack propagation and thus effectively suppressing crack initiation. Nematzadeh *et al.*[59] and Zhong *et al.*[57] reported that reducing heat input during welding significantly alleviated cracking. However, Idowu *et al.*[60] reached the opposite conclusion: when grain boundary liquation is sufficiently severe, higher heat input can enhance grain boundary ductility and consequently reduce cracking. Similarly, Bian *et al.*[61] found that moderately increasing heat input could effectively suppress crack formation during laser-forming repair of DZ125 superalloy. This is because higher heat input reduces thermal stress to some extent and increases the amount of eutectic liquid phase, promoting better feeding and enabling *in situ* healing of incipient cracks during solidification. Ebrahimnia *et al.*[62] employed a grain refinement strategy to suppress the formation of coarse γ' phases, MC carbides, and γ–γ' eutectics, successfully reducing cracking in welded IN-738LC alloy. Xu *et al.*[41] investigated the influence of induction preheating on the microstructure and cracking behavior of laser solid-formed IN738LC. The results indicated that preheating the substrate significantly reduced thermal stresses during deposition, thereby decreasing crack density in as-deposited samples. In contrast, Chen *et al.*[55] demonstrated that bottom-side directional cooling of the substrate was an effective approach for inhibiting the initiation and propagation of thermal cracks. Directional cooling enhanced the directionality of heat flow during solidification, reduced grain boundary misorientation, destabilized interdendritic liquid films, and alleviated local stress concentration. In summary, while optimization of process parameters and substrate pretreatment can both

contribute significantly to crack mitigation, they have inherent limitations and are often insufficient to eliminate cracking. Moreover, conflicting requirements among different control strategies frequently arise, resulting in an extremely narrow processing window for nickel-based superalloys.

In recent years, alloy design has emerged as an increasingly recognized and widely investigated strategy for mitigating cracking in metallic materials. A substantial body of research has been devoted to this approach. To suppress SC in laser solid-formed Inconel 625, the authors of this study implemented a hybrid alloying strategy by incorporating varying amounts of titanium (Ti).[39] The results revealed that when the Ti content in Inconel 625 was below 2 wt.%, the solidification temperature range remained relatively constant at approximately 210°C. However, with further increases in Ti content, the solidification temperature range significantly decreased. At a Ti content of 5 wt.%, the range dropped to 149°C—a reduction of 30% compared to that of the base Inconel 625 alloy. This led to a marked improvement in crack resistance; cracks were eliminated in the as-deposited samples when the Ti content exceeded 3 wt.%. This enhancement is primarily attributed to the narrowed solidification temperature range, which reduces the alloy's susceptibility to SC. In addition, the volume fraction of (γ + Laves) eutectic phases increased significantly with Ti addition, resulting in the formation of thicker interdendritic liquid films during the later stages of solidification. These thicker films enhance feeding capability and reduce the likelihood of crack initiation. When the volume fraction of interdendritic liquid exceeds 7%, the feeding channels become more continuous, enabling sufficient liquid to backfill and heal incipient cracks during solidification. It has been found that reducing the contents of minor alloying elements manganese (Mn) and silicon (Si) significantly decreased cracking in laser-additively manufactured HX superalloy.[35,36] The primary mechanism is that lowering the levels of these elements narrows the solidification temperature range, thereby reducing its propensity for SC during processing. Chen *et al.*[63] successfully reduced cracking in laser-cladded IN-738 alloy layers by incorporating small amounts of rare earth oxide ($Y_2O_3$). Han *et al.*[64] found that the addition of nano-sized TiC particles to HX effectively suppressed crack formation. This was primarily attributed to an increased volume fraction of low-angle grain boundaries and subgrain boundaries, as well as the enhanced yield strength (YS) of the alloy, which collectively improved resistance to solid-state cracking. Harrison *et al.*[56] proposed an alloy redesign strategy to mitigate microcrack formation in nickel-based superalloys during AM. Their approach focused on increasing the concentration of solid-solution strengthening elements to enhance the high-temperature strength of HX. As a result, the thermal stresses generated during fabrication were no longer sufficient to exceed the alloy's strength, thereby effectively preventing crack initiation. These studies collectively demonstrate that compositional optimization is a highly effective strategy for minimizing cracking in laser-additively manufactured components. Moreover, this approach provides a promising pathway for the future design of nickel-based superalloys specifically tailored for AM applications.

## 3. Microstructural evolution and strengthening-toughening mechanisms of nickel-based superalloys fabricated by AM

The microstructure and mechanical properties of nickel-based superalloys fabricated by AM are primarily determined by the near-rapid solidification process within the molten pool during deposition, as well as by the solid-state phase transformations occurring during subsequent thermal cycles and post-processing heat treatments. Therefore, a clear understanding of microstructural evolution during fabrication and heat treatment is a prerequisite for achieving superior mechanical performance. Unlike traditional manufacturing processes (*e.g.*, casting, forging, and powder metallurgy), AM is characterized by rapid solidification in a small molten pool and repeated thermal cycling. During solidification, the molten pool exhibits a high temperature gradient (approximately $10^6$ K/m) and a high cooling rate ($10^3$–$10^6$ K/s). Due to the heat transfer characteristics within the molten pool, the temperature gradient decreases from the bottom to the top, while the solidification rate increases, as illustrated in Figure 2C. In addition, the direction of the temperature gradient evolves from being nearly perpendicular to the scanning direction at the pool bottom to nearly parallel at the top. The growth direction of columnar grains is governed by the local heat flow direction and the crystallographic preferred orientation. Consequently, the columnar grain growth direction—perpendicular to the local temperature gradient at the pool top—shifts from perpendicular to parallel relative to the scanning direction, resulting in the formation of misoriented dendrites in the upper region of the molten pool. Furthermore, according to the columnar-to-equiaxed transition diagram for nickel-based superalloys (Figure 2D), as the temperature gradient decreases and the solidification rate increases, a transition from columnar to equiaxed grains occurs, leading to the formation of equiaxed grains in the upper region of the molten pool. When the subsequent layer is deposited, the equiaxed grain region at the top of the previous layer is remelted. Since the matrix phase of nickel-based superalloys is the γ-phase with an FCC structure, which exhibits a strong

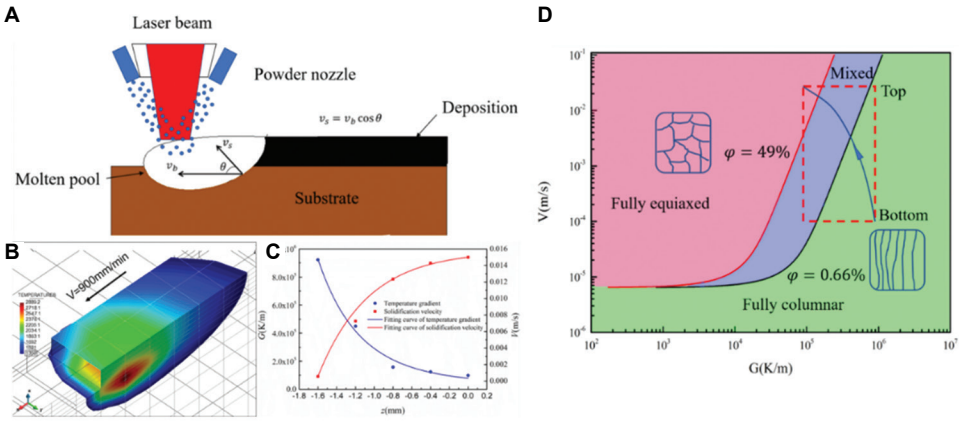


**Figure 2.** Solidification conditions of the molten pool and structure selection map for laser solid-formed Inconel 625 alloy. (A) Schematic of laser-directed energy deposition processing.[66] (B) The molten pool morphology and temperature filed of single-track; (C) Evolution of the local solidification variables G and V as the depth z for the 1st layer; (D) Microstructure selection map for Inconel 625 superalloy under the experiment conditions. Adapted with permission from Hu *et al.*[65] Copyright © 2018 Elsevier Limited

<001> crystallographic growth preference, columnar grains with non-<001> orientations are progressively eliminated during competitive growth. This enables the epitaxial growth of <001>-oriented grains across multiple deposited layers, ultimately resulting in a pronounced <001> solidification texture in the as-deposited material.[65]

The high cooling rate inherent in AM results in extremely fine dendritic substructures within the grains, and in some cases, even cellular structures may form. Although macrosegregation is generally absent in AM-processed materials, microsegregation remains significant. The segregation of alloying elements promotes the formation of interdendritic eutectic phases, which can be either dispersed or continuously distributed (Figure 3).[39] In addition, the rapid, localized heating, and cooling cycles during AM introduce substantial thermal stresses within the deposited layers. On cooling, significant residual stresses are retained, and the as-deposited samples exhibit high dislocation densities (Figure 4).[64] Therefore, the microstructure of nickel-based superalloys fabricated by AM is characterized by coarse, epitaxially grown columnar grains, containing fine dendritic or cellular substructures and high dislocation density within the grains. Eutectic phases form in the interdendritic regions to a certain volume fraction, and the material develops a strong solidification texture. Consequently, AM-fabricated nickel-based superalloys exhibit pronounced microstructural and mechanical anisotropy.[10]

The size and distribution of interdendritic eutectic phases significantly influence the strength and ductility of nickel-based superalloys. On one hand, the elements that segregate during solidification—such as Nb, Ti, and Al—are often the primary strengthening elements. The formation of interdendritic eutectic phases depletes these elements from the γ-matrix, thereby reducing the solute concentration available for precipitation hardening and ultimately lowering the alloy's overall strength. On the other hand, interdendritic eutectic phases are typically hard and brittle, acting as preferential sites for crack initiation or serving as easy paths for crack propagation under applied stress. This behavior severely compromises the alloy's fracture toughness and ductility. To achieve superior mechanical properties, precise control over the microstructure of laser-based additively manufactured nickel-based superalloys is essential. Current strategies primarily focus on optimizing processing parameters to tailor solidification conditions within the molten pool and suppress the formation of continuously networked eutectic phases. These process optimizations are typically followed by post-processing heat treatments, which further refine grain morphology and size, as well as the morphology, volume fraction, and spatial distribution of secondary precipitated phases.[65]

Extensive research has been conducted by numerous domestic and international institutions on the microstructural evolution and mechanical properties of laser-additively manufactured nickel-based superalloys with relatively good weldability, such as Inconel 718, Inconel 625, and HX.[65-77] Some additively manufactured components made from these alloys have already been successfully implemented in aerospace engines and gas turbines. Among these alloys, Inconel 625 and HX are solid-solution-strengthened superalloys, whose microstructural evolution, phase composition, and strengthening-toughening mechanisms are relatively straightforward. In contrast, Inconel 718 is a precipitation-strengthened superalloy characterized by more complex

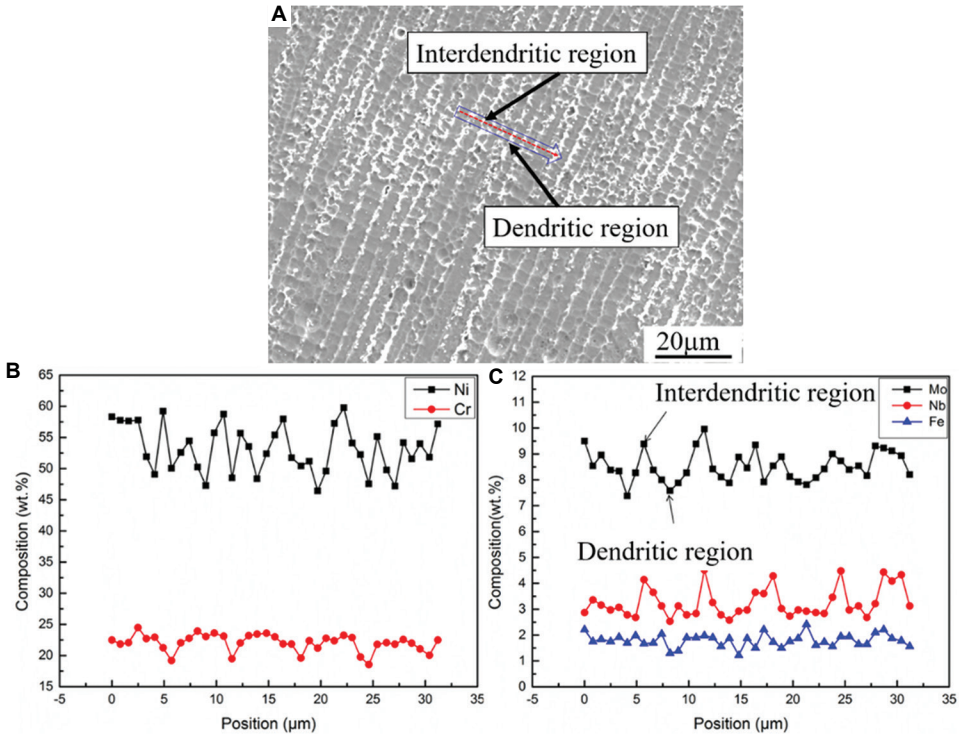


**Figure 3.** Microscale elemental segregation in the as-deposited sample of laser solid-formed Inconel 625 alloy. (A) Distribution of elements in dendritic and interdendritic region. (B) The distribution of Ni and Cr elements in the interdendritic regions and dendritic arms. (C) The distribution of Mo, Nb, and Fe elements in the interdendritic regions and dendritic arms. Adapted with permission from Hu *et al.*[39] Copyright © 2017 Elsevier Limited

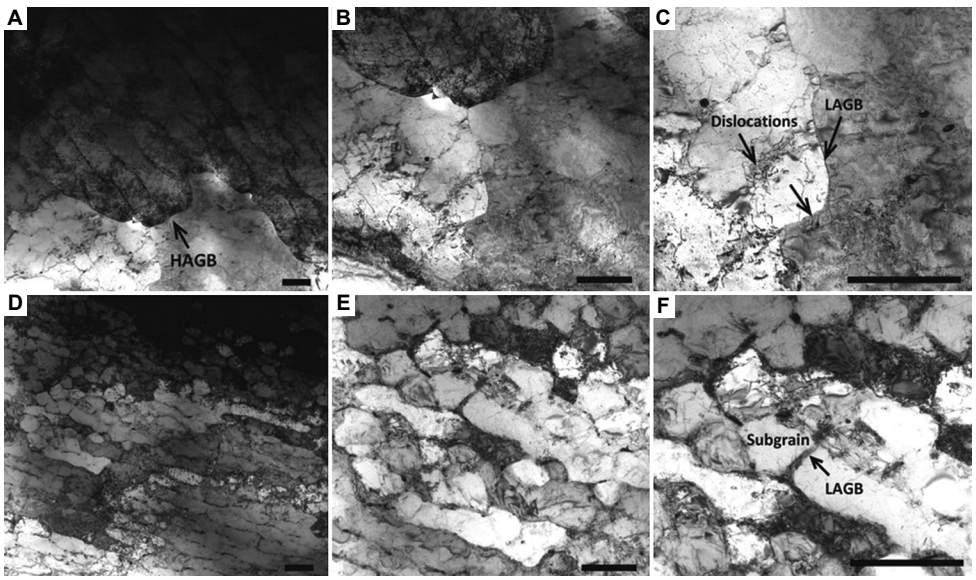


**Figure 4.** Dislocation configurations in laser-additively manufactured Hastelloy X (HX) alloy. (A-C) Transmission electron microscopy (TEM) images of the as-built HX alloy at different magnifications: Characteristic structure of high-angle grain boundaries (A), subgrain structure (B), and characteristic structure of dislocations and low-angle grain boundaries (LAGBs) (C). (D-F) TEM images of TiC nanoparticles enhanced HX sample, displaying increased dislocation density and the presence of LAGBs: Subgrain structure (D), dislocation cell (E), and characteristic structure of subgrain and LAGBs (F). Scale bars: 1 μm. Adapted with permission from Han *et al.*[64] Copyright © 2019 Elsevier Limited

phase assemblages and multi-faceted strengthening mechanisms. Despite significant progress, several critical challenges in the AM of nickel-based superalloys remain unresolved:

(i) Non-equilibrium phases, such as Laves phases, carbides, and γ–γ' eutectic phases, formed during rapid solidification in the molten pool can significantly degrade the mechanical properties of the material.
(ii) AM- fabricated nickel-based superalloys typically exhibit mechanical anisotropy and a combination of high strength with low ductility. Although post-processing heat treatments can eliminate or reduce microstructural anisotropy, anisotropic mechanical behavior often persists. Compared to their wrought counterparts, AM superalloys generally display inferior tensile ductility even after heat treatment, failing to meet stringent requirements for structural stability and operational safety.
(iii) Fatigue, creep, and long-term durability data for AM nickel-based superalloys remain limited. These materials also suffer from poor long-term plasticity, and the underlying deformation mechanisms under creep or sustained loading conditions are not yet fully understood. Consequently, the full application potential of AM nickel-based superalloys has not been fully realized.

Dinda *et al.*[78] found that the laser scanning strategy is a key factor influencing the crystallographic texture of laser-additively manufactured Inconel 718 alloy. Unidirectional laser scanning tends to promote the formation of a fiber texture, whereas bidirectional scanning results in a rotated cube texture. The difference in texture type is primarily attributed to the significant variation in temperature gradients within the melt pool induced by different scanning strategies. Ma *et al.*[79] investigated the texture of as-deposited Inconel 625 fabricated by LAM and found that it is dominated by a strong Goss texture ({011}<100>), with a weaker cube texture ({001}<100>) component. This specific texture type leads to a lower work hardening rate in the additively manufactured alloy compared to its wrought counterpart. The observed texture in Inconel 625 differs from that reported by Dinda *et al.*[78] for Inconel 718. Analysis indicates that, at a constant scanning speed, increasing the laser power and the material's absorptivity enhances the heat input, resulting in a deeper molten pool. Consequently, the temperature gradient along the deposition (z) direction decreases, and the maximum heat flow direction becomes increasingly aligned with the laser scanning direction. As a result, <100>-oriented grains are favored to grow along the scanning path, promoting the formation of a Goss texture. These findings demonstrate that process parameters—such as laser power, scanning speed, scanning strategy, and material absorptivity—exert a significant influence on texture development in laser-additively manufactured nickel-based superalloys, which, in turn, affects their mechanical anisotropy and overall performance.

For Nb-containing nickel-based superalloys, such as Inconel 625 and Inconel 718, the segregation of Nb and Mo during solidification is the primary driver for the formation of topologically close-packed (TCP) Laves phases. The presence of Laves phases significantly degrades the mechanical properties of these alloys. Studies have demonstrated that needle-like or plate-like Laves phases often act as preferential sites for crack initiation and propagation pathways, thereby substantially reducing the creep strength and room-temperature ductility of the superalloys.[80,81] When Laves phases precipitate as continuous films along grain boundaries, they can severely embrittle the interfaces and drastically reduce the creep life of the alloy.[82] In the GH2135 alloy, a small amount of fine, granular Laves phases at the grain boundaries did not significantly affect the strength or ductility. However, as the volume fraction of Laves phases increased, pronounced mechanical degradation became evident.[83] Li *et al.*,[84] in their study of the K4169 alloy, found that a large volume of coarse, blocky Laves phases led to a 20% reduction in room-temperature tensile strength and a 60% reduction in ductility. Under creep testing conditions of 650°C and 620 MPa, the alloy exhibited a 60% decrease in both creep life and creep elongation. Similarly, Sullivan *et al.*[85] reported that in Inconel 718, even a small Laves phase volume fraction of just 2–3% can lead to a significant deterioration in both strength and ductility.

Therefore, in the AM of Nb-containing nickel-based superalloys, it is essential to strictly control the size, morphology, and distribution of Laves phases. Studies have demonstrated that in laser-additively manufactured Inconel 625 alloys, as the deposition height increases, the accumulated heat in successive layers is not effectively dissipated, leading to a gradual rise in baseplate temperature. Consequently, the temperature gradient within the molten pool decreases during solidification, primary dendrite arm spacing increases, and secondary dendrite arms become more developed. This provides greater interdendritic space and longer solidification time for Laves phase formation. As a result, the size of Laves phases gradually increases from the bottom to the top of the deposited structure. This indicates that controlling the solidification conditions in the molten pool is critical to avoiding coarse and continuously distributed Laves phases in interdendritic regions. Ling *et al.*[86] found that increasing the cooling rate during solidification reduces secondary dendrite arm spacing, which effectively suppresses both the size and volume fraction of Laves phases in Inconel 718 alloys. The laser AM process inherently features high cooling rates, resulting in finer Laves phases compared to those formed during conventional casting. Xiao *et al.*[87,88] investigated the influence of quasi-continuous wave (QCW) pulsed laser

and continuous wave (CW) laser on Nb segregation, Laves phase characteristics, and mechanical properties in laser-additively manufactured Inconel 718. The results indicated that compared to continuous laser, pulsed laser operation provides higher peak cooling rates during solidification, which more effectively suppresses Nb microsegregation, reduces Laves phase size, and enhances overall mechanical performance. In addition, high-temperature solution treatment significantly affects the content, morphology, and size of Laves phases in AM Inconel 625 and Inconel 718 alloys. During solution treatment of laser-additively manufactured Inconel 625, substantial dissolution of Laves phases is observed. As the solution temperature increased, both the size and volume fraction of Laves phases decreased progressively. The dissolution kinetics of Laves phases are primarily governed by the long-range diffusion of alloying elements, such as Nb and Mo. With increasing solution temperature, the diffusion coefficients of these elements increase considerably, greatly accelerating the dissolution process. Chlebus *et al.*[68] reported that after solution treatment at 980°C and 1040°C for 1 h, Nb- and Mo-rich granular Laves phases, a small amount of MC-type carbides, and δ-phases were still present at the grain boundaries of as-built Inconel 718 samples. However, after solution treatment at 1100°C for 1 h, the δ-phase completely dissolved, large Laves phases nearly disappeared, and noticeable grain growth occurred. Tucho *et al.*[89] reported that in SLM-manufactured Inconel 718, Laves phases did not fully dissolve even after heat treatment at 1250°C for 7 h, with nanoscale remnants persisting within coarsened grains. Sui *et al.*[80] studied the effect of Laves phases on the room-temperature tensile properties of laser-additively manufactured Inconel 718 alloys. They found that Laves phases influence the YS primarily by altering the volume fraction and morphology of strengthening phases. Moreover, compared to elongated or network-like Laves phases, spherical or isolated morphologies are more favorable for plastic deformation and ductility. Therefore, by optimizing the solidification conditions in the molten pool and applying tailored solution heat treatments, it is possible to effectively regulate the morphology, size, and spatial distribution of Laves phases, thereby enhancing the mechanical properties of the alloy.

During the solution treatment of additively manufactured nickel-based superalloys, in addition to the dissolution of eutectic phases, significant microstructural evolution occurs in the morphology and size of the initial grains due to static recrystallization.[65] Studies have demonstrated that after solution treatment above 900°C, the coarse, epitaxially grown columnar grains in laser-additively manufactured Inconel 625 are gradually replaced by finer equiaxed grains. As the solution temperature increases, the volume fraction of recrystallized grains also increases. When the temperature reaches 1200°C, complete static recrystallization is achieved. Concurrently, the texture strength of the alloy decreases significantly with increasing temperature, the original <100> solidification texture formed during deposition weakens, and grain orientation becomes increasingly random. Compared with the recrystallization temperature range of conventionally forged Inconel 625 (930–1040 °C), AM Inconel 625 exhibits a higher recrystallization temperature onset. This behavior can be attributed to several factors[66]:

(i) The grain size in AM alloys is relatively large, and the grain boundary area fraction is low, resulting in fewer nucleation sites for recrystallization.
(ii) The plastic strain introduced during laser AM is generally less than 5%, which is significantly lower than the 30% strain typically experienced in forging, leading to reduced stored energy and a weaker driving force for recrystallization.
(iii) A considerable amount of Laves phase remains in the as-built microstructure, which can act as pinning points that hinder grain boundary migration during recrystallization, thereby further suppressing recrystallization kinetics.

Dinda *et al.*,[90] in their study on the microstructural evolution and thermal stability of laser-additively manufactured Inconel 625, observed that when the heat treatment temperature is below 1000°C (~3/4 $T_m$), the dendritic structures formed during the AM process remain stable. Full recrystallization only occurred at around 1200°C, indicating that AM Inconel 625 possesses high thermal stability. Kreitcberg *et al.*[91] investigated the effects of different heat treatment regimens and HIP on the microstructure and mechanical properties of selective laser-melted Inconel 625. Their results demonstrated that recrystallization occurred after post-processing and HIP, leading to the formation of equiaxed grains. In AM Inconel 625, interdendritic Laves phases were significantly dissolved during solution treatment, and the grain morphology transitioned from epitaxial columnar grains to equiaxed grains, resulting in a marked improvement in ductility. However, due to the reduction in dislocation density after recrystallization, the contribution from dislocation strengthening is diminished, leading to a decrease in the alloy's YS.

For Inconel 718 alloys, the δ-, γ"-, and γ'-phases play a critical role in determining mechanical properties. Therefore, in addition to solution treatment, aging treatment is essential to achieve sufficient strength through controlled precipitation. Figure 5 displays the precipitation-temperature-time diagram for various precipitates in

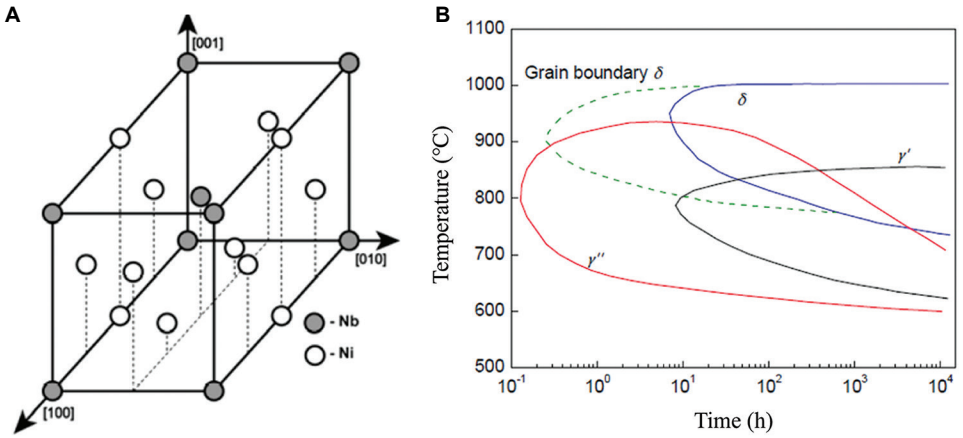


**Figure 5.** Lattice structure and precipitation kinetics curves of δ-phase. (A) Unit cell structure of the δ-phase. (B) Precipitation-temperature-time diagram of different phases in wrought Inconel 718 alloy. Adapted with permission from Thomas *et al.*[92] Copyright © 2006 Elsevier Limited

Inconel 718.[92] When the aging temperature ($T_f$) is between 870°C and 900°C, the δ phase precipitates as long needle-like particles, often continuously distributed along grain boundaries or within grains, and occasionally forming Widmanstätten structures. When 900°C < $T_f$ < 930°C, the δ phase appears as granule particles located at grain boundaries or in intragranular regions. At 940°C < $T_f$ < 960°C, it forms short rod-like morphologies preferentially along grain boundaries. At temperatures above 980°C, the δ phase is partially or completely dissolved. In laser-additively manufactured Inconel 718, the precipitation behavior of the δ-phase differs significantly from that in conventionally forged alloys. Liu *et al.*[93] investigated δ-phase precipitation in laser-additively manufactured Inconel 718 and found that, in the as-deposited condition, short needle-like or rod-like δ-phases precipitate within interdendritic regions during aging between 810°C and 950°C. After high-temperature solution treatment, elemental segregation in the interdendritic regions is substantially reduced or eliminated, and the δ-phase preferentially nucleates at high-angle grain boundaries and twin boundaries. Azadian *et al.*[94] demonstrated that both the nucleation and growth of δ-phases require a critical Nb concentration, and higher Nb content leads to an increased volume fraction of δ-phase. These studies collectively indicate that the morphology, size, and distribution of the δ-phase are strongly influenced by the degree of elemental segregation, as well as the temperature and duration of solution treatment. As presented in Table 1, the δ-phase morphology, size, and distribution vary significantly under different processing routes and heat treatment conditions.[92-97] Compared with wrought and cast alloys, the δ-phase in AM Inconel 718—under standard heat treatment—exhibits significantly finer precipitates at grain boundaries. In addition, the distribution of the δ-phase is closely correlated with the initial microstructural state of the material.

**Table 1. Morphology, size, and distribution of the δ phase under different manufacturing methods and heat treatment conditions**

| Manufacturing method | Heat treatment | Grain boundary | Intragranular |
|---|---|---|---|
| Selective laser melting | δ aging | Length: 1–2 μm<br>Width: 0.2–0.4 μm | Length: 0.5–1 μm<br>Width: 50–90 nm |
| | Homogenization+ δ aging | Length: 0.2–0.4 μm<br>Width: 10–20 nm | None |
| Wrought | δ aging | Length: 2–8 μm<br>Width: 0.2–0.5 μm | None |
| Casting | Homogenization+ δ aging | Length: 2–8 μm<br>Width: 0.5–0.9 μm | None |

At present, there are two main perspectives regarding the influence of the δ-phase on the mechanical properties of Inconel 718 alloy. The first perspective holds that the presence of the δ-phase is beneficial to the mechanical performance of Inconel 718.[98] Li *et al.*[96] found that spheroidized δ-phases distributed along grain boundaries can inhibit crack initiation and propagation during high-temperature creep and fatigue processes, thereby improving the creep ductility of the alloy while maintaining creep life. Cai *et al.*[95] suggested that a moderate amount of δ-phase can reduce the notch sensitivity of Inconel 718. Yuan *et al.*[99] also reported that short rod-shaped δ-phases can enhance both the strength and ductility of Inconel 718 at elevated temperatures. The second perspective argues that the δ-phase degrades the mechanical properties of Inconel 718.[100] Hong *et al.*[101] pointed out that Nb-depleted

zones surrounding δ-phases can reduce the low-cycle fatigue performance. Zeng *et al.*[102] observed that the YS of Inconel 718 decreases significantly with increasing δ-phase content. Zhang *et al.*[103] identified the δ-phase as the preferential site for micropore nucleation during high-temperature tensile deformation in Inconel 718, and its presence reduces the alloy's high-temperature ductility. Wang *et al.*[104] also noted that δ-phases formed along Nb-rich grain boundaries consume a large amount of Nb atoms, resulting in local compositional deviations. An excessive volume fraction of δ-phase may impair the alloy's low-cycle fatigue performance at elevated temperatures. In fact, the influence of the δ-phase on mechanical properties is strongly dependent on its morphology and volume fraction. Needle-like δ-phases hinder lateral grain boundary migration and promote intergranular fracture, leading to reduced ductility. In contrast, granular δ-phases delay necking and inhibit crack propagation, thereby enhancing the mechanical performance of Inconel 718.[105] When short rod-shaped δ-phases are present, the alloy tends to exhibit superior ductility, whereas needle-like δ-phases are associated with higher strength.[106]

The disc-shaped γ"-phase (comprising three variants), which is coherent with the matrix, along with the spherical γ'-phase, acts as the primary and secondary strengthening phases, respectively, in Inconel 718 alloy.[107] Due to a significant lattice mismatch with the γ-matrix, the γ"-phase exerts strong coherent strengthening effects and is widely recognized as the principal contributor to strength in Inconel 718.[108] Consequently, current research predominantly focuses on the evolution of the γ"-phase and its influence on mechanical properties. A. Drexler *et al.*[109] reported that the coarsening behavior of the γ"-phase in Inconel 718 can be described by the Lifshitz-Slyozov-Wagner theory. Calculations indicate that γ"-phase coarsening is governed by bulk diffusion of Nb in the γ-matrix, with an activation energy of 272 kJ/mol. Liu *et al.*[93] found that, during aging at 720°C, the growth rate of γ" precipitates in solution-treated laser additive manufactured Inconel 718 is lower than that in wrought Inconel 718. This suggests that γ" precipitates in the AM alloy exhibit superior size stability. The dimensional stability of the γ"-phase has a significant impact on the alloy's high-temperature mechanical performance. As the size of the γ" precipitates increases, they may lose coherency with the matrix, and under mechanical stress, transform into δ-phase—a transformation that degrades mechanical performance. The size of strengthening precipitates plays a crucial role in precipitation hardening. Figure 6 illustrates the interaction between dislocations and precipitates.[110] It

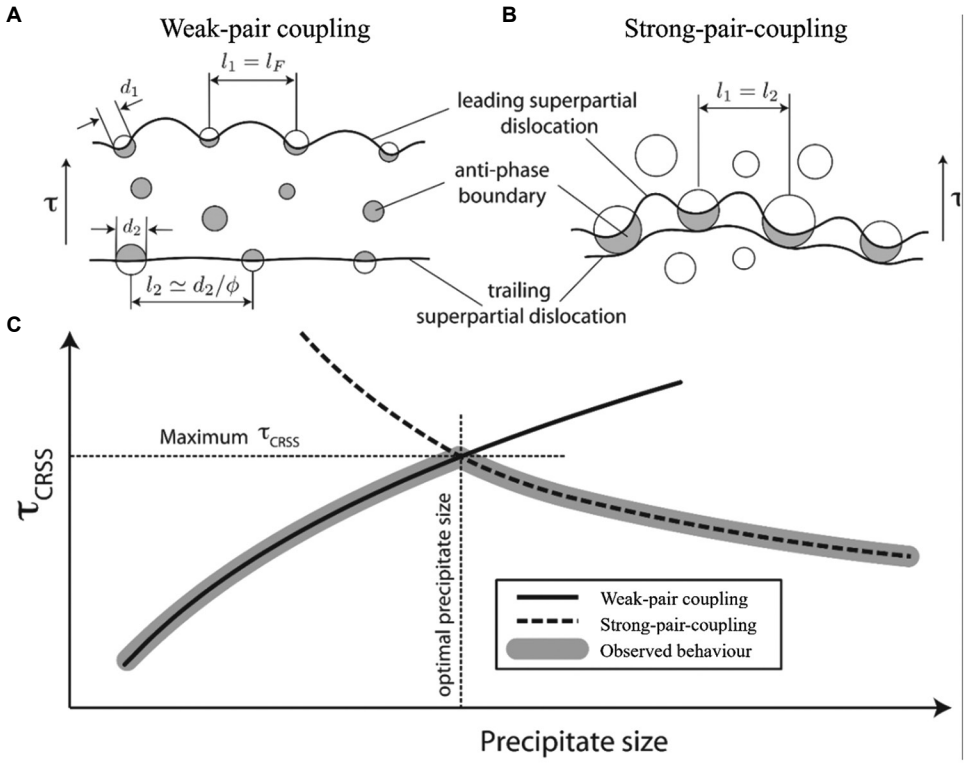


**Figure 6.** Interaction between dislocations and precipitates: (A) weak coupling; and (B) strong coupling. (C) Relationship between precipitate size and critical shear stress. Adapted with permission from Collins and Stone[110] Copyright © 2014 Elsevier Limited

can be seen that strong and weak coupling exists between dislocations and precipitates: weak coupling increases with precipitate size, while strong coupling decreases. Consequently, there exists a critical precipitate size at which the critical shear stress for dislocation cutting reaches a maximum. To determine the optimal precipitate size for strengthening in Inconel 718, numerous studies have investigated the interaction mechanisms between γ" precipitates of varying sizes and dislocations. Slama and Abdellaoui[111] suggested that the optimal γ" precipitate size in Inconel 718 is approximately 30 nm; beyond this size, the tetragonal distortion of γ" increases with particle size, leading to a reduction in strengthening efficiency. Srinivas *et al.*[112] reported that degradation in high-temperature creep resistance is closely related to the reduction of γ" size, from 23 nm to 16 nm. Ming *et al.*[113] studied the coarsening behavior of γ" precipitates in laser-additively manufactured Inconel 718 aged at 720°C for different durations and its influence on mechanical properties. The results indicated that hardness, room-temperature tensile strength, and high-temperature creep resistance of the alloy initially increase and then decrease with increasing γ" size. Chaturvedi and Han[114] indicated that the steady-state creep rate decreases as γ" particle size increases. However, once the size exceeds a critical threshold, the creep rate begins to rise again. Moreover, the particle size corresponding to the minimum creep rate is slightly smaller than that associated with peak tensile strength at room temperature. This difference arises from distinct deformation mechanisms: at room temperature, deformation is primarily governed by dislocation cutting through the precipitates, whereas at elevated temperatures, dislocation climb becomes the dominant mechanism.

From the above analysis, it is evident that the size and distribution of eutectic phases formed during the solidification of nickel-based superalloys, as well as the size, volume fraction, and spatial distribution of strengthening phases after heat treatment, all have a significant influence on the mechanical properties of the alloy. By optimizing processing parameters and subsequent heat treatment conditions, it is possible to tailor the microstructure and enhance mechanical performance. However, the selection of heat treatment procedures should fully account for the initial microstructural state of the alloy. At present, heat treatment processes for additively manufactured superalloys largely follow conventional procedures. For example, the heat treatment regime used to control the size of strengthening phases in Inconel 718 still follows the traditional two-step aging treatment developed for wrought alloys, without adequately considering the microstructural characteristics of the as-deposited condition. Liu *et al.*[93] have demonstrated that the growth kinetics of γ" precipitates differ between wrought and laser-additively manufactured Inconel 718 alloys under identical aging conditions. Furthermore, in-depth research and analysis remain limited regarding the optimization of strengthening phase size in AM nickel-based superalloys and their impact on deformation mechanisms.

Superalloy components serve for long periods under high-temperature, high-pressure, and oxidizing conditions. Their high-temperature fatigue performance, creep rupture life, creep properties, and oxidation resistance significantly influence their service life. Among these, defects, surface quality, and microstructure are key factors determining the high-temperature service performance of superalloys. Wan *et al.*[115] have investigated the effects of different thicknesses (1.3 and 3.3 mm) and surface states (as-formed and machined) on the fatigue performance of Inconel 718 alloys fabricated by LPBF. Combined with 3D high-resolution X-ray tomography (3D-XRT) and finite element analysis (FEA) simulations, the impact of surface defects on fatigue life was analyzed in depth. The results indicated that as wall thickness decreases, the material's microstructure and surface roughness undergo significant changes, leading to distinct thickness dependencies in its high-temperature fatigue strength: unmachined thin-walled samples exhibited longer fatigue life, while machined thick-walled samples exhibited the opposite trend, primarily attributed to differences in stress distribution, surface roughness, and thickness-dependent microstructure. In addition, FEA simulations revealed that the depth and shape of defects exert important effects on fatigue life; when defect sizes are small, the shape of defects reduces the material's fatigue limit more significantly than depth. Crack growth rates are significantly influenced by material microstructure, temperature, and loading direction. At 25°C, as crack length increases, the crack growth rates in different loading directions (X-, XZ-, and Z-axes) follow the order Z > X > XZ. At 650°C, this order changes to XZ > X > Z, with only a small difference between the X and XZ directions. Furthermore, crack growth rates under high-temperature conditions are significantly higher than those under low-temperature conditions, indicating a notable regulatory effect of temperature on crack propagation. The crack propagation process is accompanied by complex fracture mechanisms, including grain boundary blocking, slip activity, and secondary crack formation, all of which are closely related to the material's microstructural characteristics.[116] Yu *et al.*[117] studied the high-cycle fatigue (HCF) performance of Inconel 718 alloys fabricated by LDED at room temperature and 650°C, and explored the influence of heat treatment on the material's microstructure and mechanical properties. By adopting a specific heat treatment scheme—homogenization +

solution + aging (HSA)—the alloy's microstructure was optimized. Results indicated that Inconel 718 alloys treated with HSA exhibit a typical bimodal granular distribution, including coarse grains (CGs) and fine grains. Compared with Inconel 718 produced by traditional manufacturing methods, the fatigue limit ($\sigma_a$) of HSA-treated LDED Inconel 718 is approximately 385 MPa at room temperature and 280 MPa at 650°C, suggesting obvious temperature dependence. Further analysis indicated that as the test temperature increases, the fatigue crack initiation mode transitions from surface slip to fracture along large grain boundaries, and the presence of CGs significantly affects the material's fatigue strength.

Zhang *et al.*[118] conducted a comparative analysis of the microstructure and creep properties of Inconel 718 alloys fabricated by LPBF and forging. The results indicated that Inconel 718 fabricated by LPBF has a more complex microstructure, characterized by uneven grain size and shape, as well as the distribution of a small amount of second phases, while the forged alloy exhibits more regular grain shape and uniform grain size. This difference leads to lower average creep life, reduction of area, and uniform elongation of the LPBF alloy during the creep stage. Studies also found that in the steady creep stage, the LPBF alloy has fewer activated slip systems due to its irregular grain morphology, whereas the grains of the forged alloy can more easily activate slip systems to alleviate stress concentration. In addition, in the tertiary creep stage, the abnormal grain size distribution and shape in the LPBF alloy exacerbate stress concentration at grain boundaries, promoting the initiation and propagation of initial microcracks and thus accelerating material fracture. Subsequently, they further investigated the influence of grain boundary serration (GBS) on creep properties and its formation mechanism in Inconel 718 alloys fabricated by LPBF. By adjusting heat treatment conditions, such as intermediate solution temperature and cooling rate, different degrees of GBS were successfully achieved. Studies found that GBS significantly increases creep life by approximately 56%, increases creep strain by about 19%, and reduces creep strain rate by roughly 26%. Analysis of crack surface morphology and grain boundary dislocation density using Scanning Electron Microscopy and Electron Backscatter Diffraction confirmed that the main role of GBS in delaying crack initiation is its ability to effectively alleviate stress concentration. Further research revealed three GBS formation mechanisms: serration formation caused by the growth of δ phases along specific directions, inhibition of grain boundary migration by δ-phases larger than the critical size, and grain boundary distortion induced by element segregation.[119]

## 4. Alloy design for AM of nickel-based superalloys

There is a strong correlation among composition, processing, microstructure, and properties in materials science. In AM of nickel-based superalloys, the size and distribution of precipitates play a crucial role in determining the mechanical performance of the alloy. For instance, in laser-additively manufactured Inconel 718 and Inconel 625 alloys, the presence of chain-like Laves phases distributed in interdendritic regions not only increases the susceptibility to hot cracking but also serves as preferential sites for crack initiation and pathways for crack propagation under load, thereby significantly degrading the mechanical properties. Studies have demonstrated that during the AM process, reducing laser power, increasing scanning speed, applying active cooling to the substrate, and employing QCW laser modes can enhance the cooling rate, refine dendrite arm spacing, and promote a more uniform and dispersed distribution of precipitates within the interdendritic regions. Moreover, adjusting heat treatment temperature and holding time can modify the size and morphology of precipitates, thus improving the mechanical properties of nickel-based superalloys. However, an increase in cooling rate also leads to a significant rise in residual stress, which may induce plastic deformation or cracking and consequently compromise dimensional accuracy and structural integrity. In addition, excessively high heat treatment temperatures can result in grain coarsening, whereas overly low temperatures may prevent complete dissolution of secondary phases. These factors impose limitations on the extent to which microstructure and mechanical properties can be tailored through post-process heat treatments. Therefore, under the constraints of maintaining dimensional precision and forming quality, the potential for enhancing mechanical properties solely through optimization of processing and heat treatment parameters is inherently limited.[56]

In recent years, significant progress has been made in the AM of aluminum alloys. Researchers have developed Sc-modified Al-Mg-Sc-Zr alloy powders specifically tailored for laser-based AM, taking into account the unique thermal and solidification characteristics of AM processes. After SLM and subsequent heat treatment, these alloys exhibit excellent overall mechanical properties (with tensile strength exceeding 500 MPa and elongation surpassing 10%) and have been successfully applied in aerospace components.[120] This success demonstrates that alloy composition design aligned with the inherent characteristics of AM processes holds great potential for advancing the industrial application of nickel-based superalloys in AM.

From the above analysis, it is evident that current challenges in AM of nickel-based superalloys primarily lie in crack control during both the fabrication and post-processing stages, as well as in microstructural regulation and toughening strategies. Therefore, alloy design should first consider the influence of different alloying elements on crack initiation and propagation. Furthermore, to ensure the service performance, efforts should be made to maximize the volume fraction of strengthening phases. At present, compositional optimization of existing alloys through minor modifications has been demonstrated to reduce or even eliminate cracking to some extent, as discussed in detail in Section 2. However, there remains a lack of in-depth research on the mechanical properties of these modified alloys. Sreeramagiri *et al.*[121] combined laser AM with synchronized powder feeding, high-throughput compositional design, and phase diagram modeling to develop a novel nickel-based superalloy (WSU 150). By suppressing premature precipitation of strengthening phases during solidification, cracking was effectively avoided. A suitable heat treatment was then applied to fully precipitate the strengthening phases and enhance mechanical performance. Specifically, in the laser deposition process, two powder feeders were used to deliver Alloy A (with low γ' phase volume fraction) and Alloy B (with high γ' volume fraction) into the melt pool at a predetermined ratio, enabling *in situ* compositional synthesis. This created compositional gradients across different regions of the XY-plane in the deposited component, transitioning from Alloy A to Alloy B. Microstructural characterization and hardness testing of these gradient samples were performed to identify optimal compositions—those exhibiting no cracks and high microhardness. Through this high-throughput screening, the WSU 150 alloy (with a γ' phase volume fraction of 38%) was selected. In the as-deposited state, WSU 150 exhibited no cracking and a relatively high hardness of 375 HV. Subsequent optimization of laser deposition parameters and mechanical testing revealed that the as-deposited WSU 150 alloy achieved a YS of 867 MPa, ultimate tensile strength (UTS) of 1188 MPa, and an elongation of 27.9%. After aging at 760°C for 4 h, the yield and tensile strengths increased to 1114 MPa and 1396 MPa, respectively, while the elongation decreased to 16.1%. These room-temperature mechanical properties surpass those of Rene 88DT and indicate potential for service temperatures up to 800°C.

The alloy design strategy adopted in the study,[121] known as the element blending method, involved combining two well-established superalloys in controlled ratios for laser deposition. While this approach offers certain advantages, it also presents notable limitations. When blending two complex alloys, the concentration of multiple elements changes simultaneously, making it difficult to isolate the specific contributions of individual elements to improve cracking resistance or mechanical performance. As a result, the underlying mechanisms often remain unclear. Moreover, since nickel-based superalloys are typically employed in high-temperature environments, evaluation based solely on room-temperature tensile properties is insufficient for assessing practical applicability. More recently, Tang *et al.*[122] employed a physics-guided high-throughput computational alloy design approach to develop two AM-specific nickel-based superalloys: ABD-850AM (with ~3 wt.% Al and Ti) and ABD-900AM (with ~5 wt.% Al and Ti). These alloys were evaluated for both room- and high-temperature mechanical properties. Compared to commercial alloys, such as IN 939 and CM247LC, the newly developed alloys demonstrated superior printability and enhanced mechanical performance. The alloy design was guided by physically informed high-throughput computational models, which establish quantitative correlations between alloy composition and key mechanical properties. For AM applications, the primary design criterion is an alloy's resistance to cracking during solidification. Therefore, the Scheil non-equilibrium solidification model was used to calculate solidification temperature ranges, and the alloys' susceptibility to SAC during thermal cycling and heat treatment was also assessed. To ensure high mechanical performance and thermal stability, YS and creep resistance were predicted by considering key microstructural parameters, including anti-phase boundary energy, γ' phase volume fraction, and elemental interdiffusion coefficients. In addition, the tendency for TCP phase formation was evaluated using d-electron band theory. Based on these multi-objective criteria, two promising alloy compositions were identified, as displayed in Figure 7. The ABD-850AM alloy was selected for experimental validation and compared with IN 939 and CM247LC.[122]

Results indicated that ABD-850AM exhibited superior printability (*i.e.*, enhanced crack resistance) and reduced texture intensity. As illustrated in Figure 8, the ABD-850AM samples were free of cracks, whereas the other two alloys frequently exhibited SC, LC, and SAC. Research by Kou[123] on SC pointed out that evaluating crack susceptibility based solely on the solidification temperature range is limited, as it neglects the alloy's solidification path during the final stages. He proposed a new evaluation metric—Solidification Cracking Index—which integrates both the strain rate in the solid phase and the feeding capability of the residual liquid phase to assess the likelihood of SC. Tensile tests across a range of temperatures were conducted to evaluate the alloys' susceptibility to hot ductility loss and SAC. The high-temperature tensile and creep properties of ABD-900AM

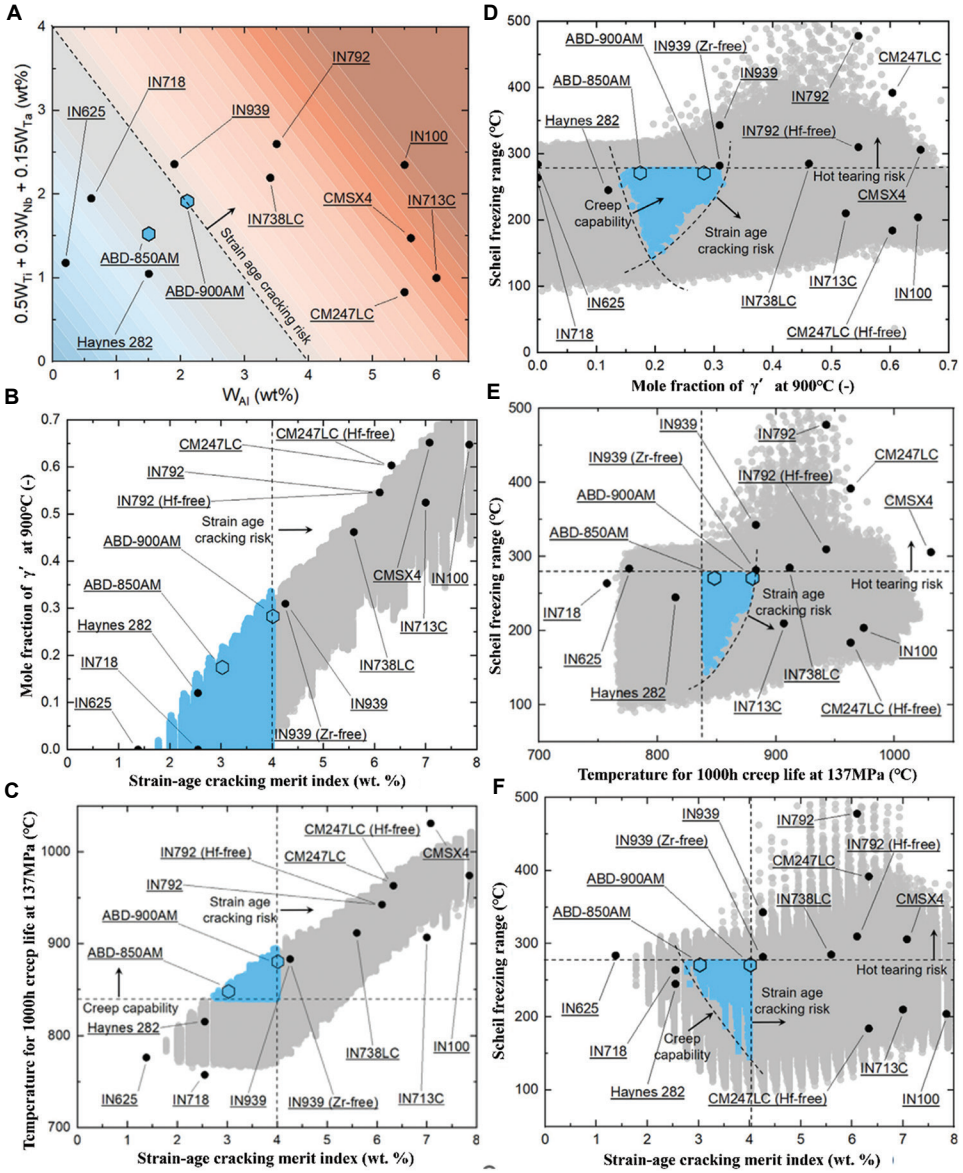


**Figure 7.** Composition screening of nickel-based superalloys. (A) Modified weldability diagram with maximum strain-age cracking index identified. (B and C) Strain-age cracking merit index and its relationship to γ' fraction (B) and creep merit index (C). (D and E) Magnitude of freezing range in relation to γ' fraction (D) and creep merit index (E), where strain-age cracking and creep merit contours are indicated. (F) Final design space used to isolate new grades of alloy based on freezing range, strain-age cracking index, and minimum required strength and creep. Adapted with permission from Tang *et al.*[122] 

demonstrated excellent strength and ductility, with creep performance significantly surpassing that of IN 718 and approaching that of CM247LC. The study comprehensively evaluated the printability and mechanical performance of AM-specific nickel-based superalloys, providing valuable insights and strategic guidance for future design of alloy compositions tailored for AM.

Liang *et al.*[124] utilized coaxial powder-fed laser AM technology to develop a novel nickel-based superalloy (ZK401), characterized by low crack susceptibility, low density, and high strength, and obtained a corresponding patent. According to the patent, this alloy is primarily intended for the repair of high-temperature alloy components and for the AM of medium- and low-temperature nickel-based alloy parts. The alloy composition includes Al, Ti, and Nb as key precipitation-strengthening elements that promote γ' phase formation; Cr, Mo, and Co as solid-solution strengthening elements; and Si, C, and Hf as grain boundary-strengthening elements. Cr plays

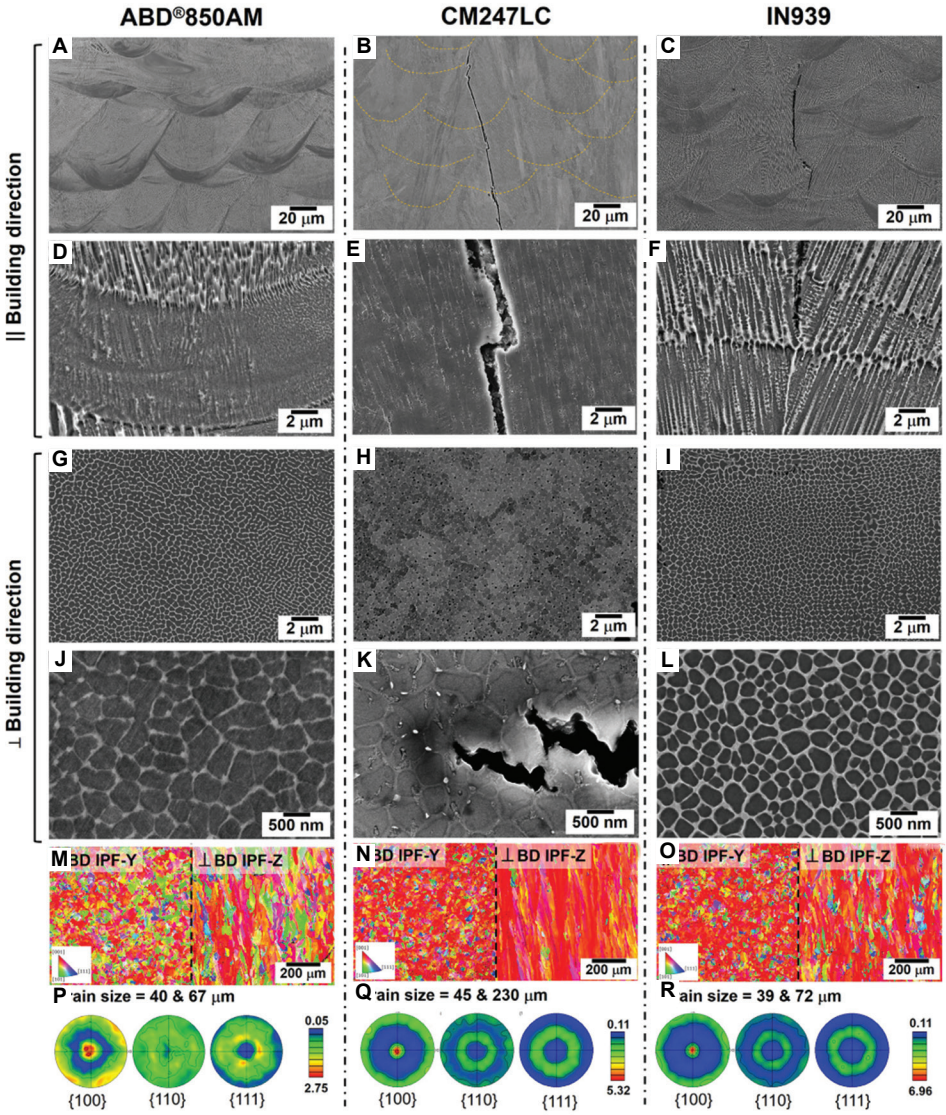


**Figure 8.** Microstructure comparison of additively manufactured ABD850AM, CM247LC, and IN939 alloys. (A-F) Microstructure of the XZ-plane at two magnifications (×100 and ×1000). (G-L) Microstructure of XY-plane at two magnifications. (M-O) Inverse pole figure of both planes along the building direction. (P-R) Bulk texture strength of {1 0 0}, {1 1 0}, and {1 1 1} poles. Adapted with permission from Tang *et al.*[122] Copyright © 2021 Elsevier Limited

a key role in oxidation resistance, corrosion resistance, and solid-solution strengthening. In addition, it can form carbides with C to enhance precipitation strengthening. To suppress the formation of TCP phases, the Cr content is controlled within the range of 9.0–11.0 wt.%. Mo increases the lattice misfit between the matrix and the strengthening phase, enhances atomic bonding strength, and promotes dislocation network formation, thereby improving both printability and mechanical performance.

However, excessive Mo promotes TCP phase formation, which is detrimental to oxidation and corrosion resistance. Therefore, its content is limited to 4.0–6.0 wt.%. Co contributes to solid-solution strengthening and reduces the stacking fault energy, thus improving the alloy's intermediate-temperature mechanical properties and structural stability. Its content is maintained between 9.0 and 11.0 wt.%. Nb acts as the primary strengthening element and also enhances oxidation and corrosion resistance. Nevertheless, excess Nb can promote TCP phase formation; thus, its content is controlled within 3.0–5.0 wt.%. Al is the main constituent of the γ' phase; its concentration directly determines the γ'-phase and improves oxidation resistance. However, excessive Al may lead to the formation of low-melting-point eutectic phases, which negatively affect printability. Thus, Al is maintained within 3.0–5.0 wt.%. Ti can substitute for Al in the γ'-phase

and serves as a major precipitation-strengthening element. It also enhances resistance to hot corrosion, though it may impair oxidation resistance. Its content is kept between 1.0 and 2.0 wt.%. Si improves oxidation and corrosion resistance but can form brittle $Nb_3Si$ phases when combined with Nb, thereby reducing mechanical performance. Thus, its content is limited to 0.0–0.6 wt.%. C aids in deoxidation during melting, improves melt fluidity, and forms grain boundary-stabilizing carbides. However, excessive C increases crack susceptibility; thus, its content is strictly controlled within 0.0–0.02 wt.%. Sun *et al.*[125] have revealed that in the AM of IN738LC alloy, a moderate increase in C content can improve its mechanical properties to a certain extent, particularly in terms of hardness. Nevertheless, excessive C content will instead reduce the alloy's high-temperature performance and introduce new defects. Hf enhances precipitate strengthening, purifies grain boundaries, prevents sulfur-induced embrittlement, broadens the solidus-liquidus temperature range, improves melt fluidity, and reduces SC tendency, thereby significantly enhancing weldability. Hf content is maintained within 0.1–0.6 wt.%. This alloy exhibits superior room- and intermediate-temperature tensile properties compared to Inconel 625: at room temperature, tensile strength > 900 MPa, elongation>10.0%; at 650°C, tensile strength >800 MPa, elongation>10.0%; at 800°C: tensile strength >680 MPa, elongation>7.0%. In terms of creep performance, the alloy achieves: creep life >50 h at 650°C/690 MPa; and creep life >25 h at 800°C/400 MPa. Moreover, the alloy demonstrates excellent oxidation resistance at 800°C, with no observable weight gain or spallation after prolonged exposure.[125]

The aforementioned studies are based on alloying strategies for material design, whereby increasing the content of precipitation-strengthening elements, such as Al, Ti, and Nb—followed by appropriate heat treatment—can effectively enhance the volume fraction of γ'- and γ"-strengthening phases in the alloy, thereby improving its mechanical properties. However, when the Al and Ti contents exceed 6 wt.%, the weldability of the alloy deteriorates significantly. During the AM process, this leads to a marked susceptibility to hot cracking, which adversely affects the geometric fidelity and structural integrity of the fabricated components. Therefore, improvements in the mechanical performance of AM nickel-based superalloys through alloying approaches are inherently constrained by the alloy's processability limitations.[124] Studies have demonstrated that incorporating nanoscale reinforcements—such as metal oxides, ceramic particles, and carbon-based nanomaterials—into nickel-based superalloys to form metal matrix composites (MMCs) can significantly enhance strength while maintaining favorable processability.[126,127] This strategy offers an alternative and effective pathway for enhancing the mechanical performance of laser-additively manufactured nickel-based superalloys.

Research indicates that the addition of nanoparticles reduces the thermal conductivity of the melt pool, thereby inhibiting heat transfer to the substrate. Meanwhile, the nanoparticles increase the viscosity of the molten alloy and suppress thermocapillary flow, which, in turn, reduces thermal convection within the melt pool. As a result, the HAZ is minimized, while the fusion zone is enlarged.[126] Gu *et al.*[126-129] systematically investigated multi-phase reinforcement and gradient-interface synergistic toughening mechanisms in particle-reinforced nickel-based superalloys fabricated by LAM. Their studies revealed that the addition of nanoscale TiC particles to Inconel 625 refined the grain structure. The TiC nanoparticles effectively impeded dislocation motion, resulting in a notable increase in tensile strength without compromising ductility, and also improved the alloy's tribological performance. The incorporation of nanoscale $TiB_2$ particles into Inconel 625 effectively pinned grain boundaries and suppressed grain boundary migration during deformation, thereby enhancing mechanical properties.[130] Yang *et al.*[131] systematically investigated the effects of adding 10 vol.% micron-sized TiCN particles on the microstructure and mechanical properties of Inconel 718 matrix composites fabricated through LPBF and further analyzed the performance changes of the composites after heat treatment. The results indicated that the incorporation of TiCN particles significantly improved the hardness, tensile strength, and wear resistance of the composites. In addition, heat treatment further enhanced the mechanical properties of the composites, with the improvement in compressive strength being particularly prominent. Gruber *et al.*[132] revealed that the addition of an appropriate amount of micron-sized carbides and nitrides to Inconel 718 alloy can significantly alter its macro morphology and microstructure, resulting in finer grain sizes and uniformly distributed second-phase particles. By adjusting process parameters to precisely control the type, content of additives, and the processing procedure, the mechanical properties of the material can be significantly improved while ensuring good machinability, with particular enhancement in the balance between strength and ductility. The addition of CNTs into AM nickel-based superalloys also contributed to grain refinement and strength improvement. However, it was accompanied by a reduction in ductility. After appropriate heat treatment, the composites exhibited superior overall mechanical properties compared to their unreinforced counterparts.[133] Furthermore, in Inconel 718, CNTs provided dispersion

strengthening, reduced localized strain accumulation between dendrites during solidification, and enhanced resistance to thermal stress and strain in the interdendritic regions, thereby effectively suppressing crack formation.[55]

These findings suggest that nanoparticles, as reinforcing agents, can significantly enhance alloy strength. However, this often comes at the expense of ductility, which poses significant challenges for effective toughening strategies. Therefore, there is an urgent need to explore novel reinforcing agents capable of simultaneously enhancing both strength and ductility.[134,135] Graphene, as an emerging reinforcement in MMCs, offers a high aspect ratio (lateral dimension to thickness), an exceptionally large specific surface area, and outstanding intrinsic mechanical strength. Even at low volume fractions, graphene can dramatically improve the comprehensive performance of composites, resulting in high reinforcement efficiency. Its large surface area enables superior wettability with metallic matrices compared to CNTs, promoting stronger interfacial bonding. Moreover, graphene effectively suppresses grain growth in the matrix with minimal disruption to intergranular spacing, thereby enhancing stress transfer efficiency. The surface of graphene exhibits a unique wrinkled morphology, which flattens under applied stress, dissipating energy and contributing to simultaneous improvements in both strength and toughness.[134,135] Xiao *et al.*[135] employed laser cladding to fabricate graphene-reinforced Inconel 625 composites. The resulting material exhibited increased hardness, enhanced thermal conductivity, and improved tribological performance, attributed to the self-lubricating effect of the graphene interlayer. Xiao *et al.*[135] incorporated 1 wt.% graphene into AM Inconel 718 and reported that the YS and UTS increased by 42% and 53%, respectively, compared to the unreinforced alloy. In addition, the friction coefficient and wear rate were reduced by 22.4% and 66.8%, respectively. Therefore, graphene serves as a highly effective reinforcement, capable of significantly improving both the mechanical and tribological properties of additively manufactured nickel-based superalloys.

## 5. Conclusion

The development of AM technology has liberated design constraints, making it possible to realize complex, lightweight, and functional designs and the manufacturing of engine components. This advancement has significantly contributed to the development of next-generation aerospace engines and gas turbines. At present, certain AM-fabricated nickel-based superalloy components have already been successfully installed in engines or passed rigorous qualification tests, achieving remarkable results. These milestones demonstrate the tremendous potential of AM technology in the aerospace propulsion field. However, several critical challenges remain in the AM of nickel-based superalloys, including the mitigation of process-induced defects (such as porosity and hot cracking), the precise control of microstructure evolution and resultant mechanical properties, and the design of AM-specific alloy compositions tailored to the unique thermal and solidification conditions of AM processes. Looking ahead, several key research directions warrant focused investigation and development in the field of AM nickel-based superalloys:

(i) The innovative structural design of nickel-based superalloy components leveraging AM enables lightweight, functionally integrated architecture and the fabrication of highly complex engine parts, thereby enhancing their service performance and multifunctional capabilities. With the continuous advancement of AM technology, achieving structural-functional integration in high-temperature components—while simultaneously improving the mechanical properties and service temperature of nickel-based superalloys—has become a critical development trend for meeting the demanding operational requirements of aerospace engines and gas turbines. AM offers unparalleled advantages over conventional manufacturing methods in fabricating complex geometries and enabling multi-material integration. By integrating AM with advanced design methodologies—such as topology optimization, biomimetic structures, architected metamaterials, and hierarchical architectures—the structural efficiency and material performance of components can be maximized. Therefore, structural innovation, functional design, and precise process control through AM represent key research and development directions for achieving structural-functional integration in nickel-based superalloy components for aero-engine and gas turbine applications.

(ii) In integrated components of engines and gas turbines—such as compressor disks and turbine hubs—different regions are subject to markedly distinct service conditions (*e.g.*, temperature, loading), resulting in non-uniform distributions of thermal and mechanical stresses within the material. Traditional monolithic components are increasingly incapable of meeting the demanding performance requirements in such complex operational environments. Through functionally graded material (FGM) design, the blade section can be tailored to exhibit high ductility, excellent thermal stability, and superior HCF resistance at elevated temperatures, while the disk section can be engineered for high creep resistance, low-cycle fatigue strength, and enhanced fracture

toughness. By establishing a gradual transition in mechanical and thermal performance between the disk and blade regions—aligned with the spatial variations in temperature and mechanical load—the full material and structural potential of nickel-based superalloys can be exploited. This enables the fulfillment of region-specific thermal and mechanical demands, thereby improving overall engine efficiency and reliability. AM, with its layer-by-layer, point-by-point fabrication principle, offers a unique capability to produce complex-shaped components with spatially tailored property gradients. This is achieved through *in situ* feeding of multiple materials with varying compositions, coupled with real-time adjustment of processing parameters based on predefined material and performance specifications. As a result, components with precisely controllable gradients in compositions, microstructures, and mechanical properties can be manufactured. The integration of AM with functionally graded material design represents a highly promising pathway toward the development of next-generation, high-performance gradient material components for the hot sections of aerospace engines.

(iii) Traditional strengthening mechanisms, such as grain refinement, solid solution strengthening, precipitation strengthening through dispersed phases, and deformation strengthening, can effectively enhance the strength of metallic materials. However, these approaches often sacrifice ductility and toughness, making it challenging to achieve an optimal balance between strength and plasticity. In recent years, studies have demonstrated that heterogeneous composite architectures—such as those with hybrid, layered, gradient, bimodal, hierarchical, or harmonic structures—are more effective in harnessing the synergistic coupling effects among distinct microstructural constituents. This enables the simultaneous enhancement of both strength and ductility, thereby achieving a superior combination of mechanical properties. Metal AM provides a powerful platform for fabricating complex-shaped functionally graded components with spatially controlled gradients in compositions, microstructures, and properties. This capability greatly facilitates the design and realization of tailored composite architectures for concurrent strengthening and toughening. Without modifying the base alloy composition, AM can precisely control microstructural features, including grain morphology, size, crystallographic orientation, and substructures, across different regions of the component. This enables the construction of engineered "heterogeneous" architectures that fully exploit the performance potential of conventional structural metals to meet increasingly demanding industrial requirements. Such advancements are expected to accelerate the engineering deployment of laminated and architected metal composites in aerospace and related high-performance sectors. Therefore, composite-architecture-based strengthening and toughening of AM-fabricated nickel-based superalloys represents a significant and promising research direction.

(iv) Alloy composition design for AM-specific nickel-based superalloys and nickel-based composites presents a critical research frontier. First, suitable compositions and phase constituents must be carefully selected to suppress the formation of processing defects, such as solidification and LC during both the fabrication and post-processing stages. Concurrently, the alloy must meet stringent service performance requirements under high-temperature and high-stress conditions. By integrating computational materials design software—such as Thermo-Calc and JMatPro for thermodynamic calculations, and DICTRA for kinetic simulations—with high-throughput experimental approaches, it becomes feasible to quantitatively predict the influence of elemental additions on the processability and mechanical behavior of nickel-based superalloys. This integrated approach enables rapid screening and identification of promising alloy compositions with tailored properties, thereby accelerating the development of next-generation AM-specific superalloys. Likewise, the incorporation of secondary phase particles (such as ceramic particles, rare earth oxides, graphene, and CNTs) into nickel-based superalloys offers an alternative strategy for performance enhancement. Research in this domain focuses on elucidating how these reinforcing phases affect microstructural evolution and mechanical response. However, in composite materials, the dispersion homogeneity of the secondary phase and the integrity of interfacial bonding are critical factors that significantly influence overall mechanical performance. To address these challenges, *in situ* characterization techniques—such as high-speed synchrotron X-ray radiography and small-angle neutron scattering (SANS)—can be employed to probe the dynamic behavior and spatial distribution of reinforcing phases, the initiation and propagation of metallurgical defects, and the underlying mechanisms of microstructural evolution. Such real-time insights are essential for deepening the fundamental understanding of formation and performance optimization in AM-fabricated nickel-based

composites. Consequently, AM process engineering is fundamentally distinct from conventional material processing. Therefore, the development of nickel-based superalloys and composite materials specifically engineered to leverage the unique thermal and kinetic conditions of AM processes represents a pivotal direction for future research.

## Acknowledgments

None.

## Funding

This work was supported by the Advanced Materials-National Science and Technology Major Project (Grant No. 2024ZD0601000), National Natural Science Foundation of China (Grant No. 52105344), Natural Science Foundation of Guangdong Province (Grant No. 2021A1515010942), and Guangzhou Basic and Applied Basic Research (Grant No. 202201010365).

## Conflicts of interest

The authors declare no financial or personal relationships with other people or organizations that can inappropriately influence the present work. There is no professional or other personal interest of any nature or kind in any product, service, or company that could be construed as influencing the work presented in, or the review of, the present article.

## Authors' contributions

*Conceptualization:* Yunlong Hu
*Investigation:* Zihong Wang, Qiang Zhang, Shan Li
*Methodology:* Xin Zhang
*Writing–original draft:* Yunlong Hu, Zihong Wang, Qiang Zhang, Shan Li
*Writing–review and editing:* Xin Zhang Weidong Huang

## Ethics approval and consent to participate

Not applicable.

## Consent for publication

Not applicable.

## Availability of data

Not applicable.

## References

1. Zhang Z, Huang H, Zhang Z. A review of the microstructure and properties of superalloys regulated by magnetic field. *J Mater Res Technol*. 2024;30:9285-9317.

   doi: 10.1016/j.jmrt.2024.05.189

2. Gudivada G, Pandey AK. Recent developments in nickel-based superalloys for gas turbine applications: Review. *J Alloys Comp*. 2023;964:171128.

   doi: 10.1016/j.jallcom.2023.171128

3. Ding W, Miao Q, Li B, *et al*. Review on grinding technology of nickel-based superalloys used for aero-engine. *J Mech Eng*. 2019;55:189-215.

   doi: 10.3901/JME.2019.01.189

4. Su J, Ng WL, An J, Yeong WY, Chua CK, Sing SL. Achieving sustainability by additive manufacturing: A state-of-the-art review and perspectives. *Virtual Phys Prototyp*. 2024;19(1):2438899.

   doi: 10.1080/17452759.2024.2438899

5. Tan C, Li R, Su J, *et al*. Review on field assisted metal additive manufacturing. *Int J Mach Tools Manuf*. 2023;189:104032.

   doi: 10.1016/j.ijmachtools.2023.104032

6. Su J, Li Q, Teng J, *et al*. Programmable mechanical properties of additively manufactured novel steel. *Int J Extreme Manuf*. 2025;7:015001.

   doi: 10.1088/2631-7990/ad88bc

7. Pusateri V, Hauschild MZ, Kara S, Goulas C, Olsen SI. Quantitative sustainability assessment of metal additive manufacturing: A systematic review. *CIRP J Manuf Sci Technol*. 2024;49:95-110.

   doi: 10.1016/j.cirpj.2023.12.005

8. Sarac Yakupoglu T. The qualification of the additively manufactured parts in the aviation industry. *Am J Aerosp Eng*. 2019;6(1):1-10.

   doi: 10.11648/j.ajae.20190601.11

9. CFM International. *CFM International Celebrates $32 Billion in New Orders and Commitments at 2017 Paris Air Show*. United States: CFM International; 2017.

10. Mostafaei A, Ghiaasiaan R, Ho IT, *et al*. Additive manufacturing of nickel-based superalloys: A state-of-the-art review on process-structure-defect-property relationship. *Prog Mater Sci*. 2023;136:101108.

    doi: 10.1016/j.pmatsci.2023.101108

11. Shi F, Zhao J, Wang Z, *et al*. Research on processing technology of superalloy K465 via laser additive manufacturing. *Mech Sci Technol Aerospace Eng*. 2017;36:1298-1302.

    doi: 10.13433/j.cnki.1003-8728.2017.1298

12. Wang XH, Lin X, Yang HO, *et al*. Research on the crack predictions in K465 superalloy by laser remelting based on BP neural networks. *Yingyong Jiguang/Appl Laser Technol*. 2014;34(1):9-14.

13. He B, Li D, Zhang A, *et al*. Influence of oxidation on the cracks of DZ125L nickel-based superalloy thin-walled parts in laser metal direct forming. *Rapid Prototyp J*.

2013;19(6):446-451.

doi: 10.1108/RPJ-12-2011-0133

14. Li Y, Chen K, Tamura N. Mechanism of heat affected zone cracking in Ni-based superalloy DZ125L fabricated by laser 3D printing technique. *Mater Des*. 2018;150:171-181.

doi: 10.1016/j.matdes.2018.04.032

15. Boswell JH, Clark D, Li W, Attallah MM. Cracking during thermal post-processing of laser powder bed fabricated CM247LC Ni-superalloy. *Mater Des*. 2019;174:107793.

doi: 10.1016/j.matdes.2019.107793

16. Kalentics N, Farrokhpour N, Logé RE, *et al*. Healing cracks in selective laser melting by 3D laser shock peening. *Addit Manuf*. 2019;30:100881.

doi: 10.1016/j.addma.2019.100881

17. Chen M, Hua L, Hu Z, Dong K, Qin X. Cracking and suppression mechanisms of directed energy deposited IN738 superalloy revealed by microstructural characterization, *in-situ* thermal monitoring, and numerical simulations. *J Alloys Comp.* 2025;1020:179446.

doi: 10.1016/j.jallcom.2025.179446

18. Perevoshchikova N, Gharbi F, Audinot JN, *et al*. Optimisation of selective laser melting parameters for the Ni-based superalloy IN-738 LC using Doehlert's design. *Rapid Prototyp J*. 2017;23(5):881-892.

doi: 10.1108/RPJ-04-2016-0063

19. Duan RX, Huang BY, Liu ZM, Peng K, Lu XQ. Selective laser melting fabrication and cracking behavior of Rene104 nickel-based superalloy. *Trans Nonferrous Metals Soc China*. 2018;28(8):1568-1578.

doi: 10.19476/j.ysxb.1004.0609.2018.08.10

20. Yang J, Li F, Wang Z, Zeng X. Cracking behavior and control of Rene 104 superalloy produced by direct laser fabrication. *J Mater Process Technol*. 2015;225:229-239.

doi: 10.1016/j.jmatprotec.2015.06.002

21. Carter LN, Martin C, Withers PJ, Attallah MM. The influence of the laser scan strategy on grain structure and cracking behaviour in SLM powder-bed fabricated nickel superalloy. *J Alloys Comp.* 2014;615:338-347.

doi: 10.1016/j.jallcom.2014.06.172

22. Zhao X, Chen J, He F, Tan H, Huang W. Cracking mechanism of Rene88DT superalloy by laser rapid forming. *Rare Metal Mater Eng*. 2007;36(2):216-220.

23. Bi G, Sun CN, Chen HC, Ng FL, Ma CCK. Microstructure and tensile properties of superalloy IN100 fabricated by micro-laser aided additive manufacturing. *Mater Des*. 2014;60:401-408.

doi: 10.1016/j.matdes.2014.04.020

24. Chen Y, Zhang K, Huang J, Hosseini R, Li Z. Characterization of heat affected zone liquation cracking in laser additive manufacturing of Inconel 718. *Mater Des*. 2015;90:586-594.

doi: 10.1016/j.matdes.2015.10.155

25. Chen Y, Lu FG, Zhang K, *et al*. Dendritic microstructure and hot cracking of laser additive manufactured Inconel 718 under improved base cooling. *J Alloys Comp.* 2016;670:312-321.

doi: 10.1016/j.jallcom.2016.01.250

26. Lu YZ, Lei WN, Ren WB, Chen SX. Crack analysis and control of laser cladding Inconel 718 alloy. *Surf Technol*. 2020;49(9):233-243.

27. Zhang YC, Wang Z, Zhang YY, *et al*. Microstructure, mechanical properties and thermal crack behavior of laser cladded In718 alloy coating. *J Xihua Univ* (*Nat Sci Ed*). 2022;41(3):42-50.

28. Zhang J, Li S, Wei QS, Shi Y, Wang L, Guo L. Cracking behavior and inhibiting process of Inconel 625 alloy formed by selective laser melting. *Chin J Rare Metals*. 2015;39(11):961-966.

doi: 10.13373/j.cnki.cjrm.2015.11.001

29. Qiu C, Chen HX, Liu Q, Yue S, Wang HM. On the solidification behaviour and cracking origin of a nickel-based superalloy during selective laser melting. *Mater Character*. 2019;148:330-344.

doi: 10.1016/j.matchar.2018.12.032

30. Darabi R, Oliveira JP, Nemati N, Reis A, Cesar de Sá J. Benchmarking advanced multiphase field modeling of Inconel 625 in additive manufacturing: Correlating powder bed fusion with dendrite growth and crack formation. *Materialia*. 2025;40:102384.

doi: 10.1016/j.mtla.2025.102384

31. Pakniat M, Ghaini FM, Torkamany MJ. Hot cracking in laser welding of Hastelloy X with pulsed Nd: YAG and continuous wave fiber lasers. *Mater Des*. 2016;106:177-183.

doi: 10.1016/j.matdes.2016.05.124

32. Han Q, Gu Y, Soe S, Lacan F, Setchi R. Effect of hot cracking on the mechanical properties of Hastelloy X superalloy fabricated by laser powder bed fusion additive manufacturing. *Optics Laser Technol*. 2019;124:105984.

doi: 10.1016/j.optlastec.2019.105984

33. Hu J, Lin X, Hu Y. High wear resistance and strength of Hastelloy X reinforced with TiC fabricated by laser powder bed fusion additive manufacturing. *Appl Surf Sci*. 2024;648:159004.

doi: 10.1016/j.apsusc.2023.159004

34. Han Q, Mertens R, Montero-Sistiaga ML, *et al*. Laser powder bed fusion of Hastelloy X: Effects of hot isostatic pressing and the hot cracking mechanism. *Mater Sci Eng A*. 2018;732:228-239.

doi: 10.1016/j.msea.2018.07.008

35. Hu J, Hu Y, Lan C, *et al*. Cracking mechanism and control of Hastelloy X prepared by laser powder bed fusion. *J Mater Res Technol*. 2022;21:3526-3547.

    doi: 10.1016/j.jmrt.2022.10.164

36. Tomus D, Rometsch PA, Heilmaier M, Wu X. Effect of minor alloying elements on crack-formation characteristics of Hastelloy-X manufactured by selective laser melting. *Addit Manuf*. 2017;16:65-72.

    doi: 10.1016/j.addma.2017.05.006

37. Saarimäki J, Lundberg M, Moverare JJ, *et al*. Characterization of Hastelloy X produced by laser powder bed additive manufacturing. In: *Proceedings of the World Congress on Powder Metallurgy & Particulate Materials (World PM2016)*. Hamburg, Germany: European Powder Metallurgy Association (EPMA); 2016. p. 1-8.

38. Dupont JN, Lippold JC, Kiser SD. *Welding Metallurgy and Weldability of Nickel-Based Alloys*. Hoboken, NJ: John Wiley & Sons, Inc.; 2009.

39. Hu YL, Lin X, Yu XB, Xu JJ, Lei M, Huang WD. Effect of Ti addition on cracking and microhardness of Inconel 625 during the laser solid forming process. *J Alloys Comp*. 2017;711:267-277.

    doi: 10.1016/j.jallcom.2017.03.355

40. Sonar T, Balasubramanian V, Malarvizhi S, Venkateswaran T, Sivakumar D. An overview on welding of Inconel 718 alloy - Effect of welding processes on microstructural evolution and mechanical properties of joints. *Mater Character*. 2021;174:110997.

    doi: 10.1016/j.matchar.2021.110997

41. Xu JJ, Lin X, Guo PF, *et al.* The initiation and propagation mechanism of the overlapping zone cracking during laser solid forming of IN-738LC superalloy. *J Alloys Compd*. 2018;749:859-870.

    doi: 10.1016/j.jallcom.2018.03.366

42. Cloots M, Uggowitzer PJ, Wegener K. Investigations on the microstructure and crack formation of IN738LC samples processed by selective laser melting using Gaussian and doughnut profiles. *Mater Des*. 2016;89:770-784.

    doi: 10.1016/j.matdes.2015.10.027

43. Ci S, Liang J, Li J, *et al*. Microstructure and stress-rupture property of DD32 nickel-based single crystal superalloy fabricated by additive manufacturing. *J Alloys Compd*. 2021;854:157180.

    doi: 10.1016/j.jallcom.2020.157180

44. Zhou Z, Gill AS, Qian D, *et al*. A finite element study of thermal relaxation of residual stress in laser shock peened IN718 superalloy. *Int J Impact Eng*. 2011;38(7):590-596.

    doi: 10.1016/j.ijimpeng.2011.02.006

45. Moat RJ, Pinkerton AJ, Li L, Withers PJ, Preuss M. Residual stresses in laser direct metal deposited Waspaloy. *Mater Sci Eng A*. 2011;528(6):2288-2298.

    doi: 10.1016/j.msea.2010.12.010

46. Nadammal N, Cabeza S, Mishurova T, *et al*. Effect of hatch length on the development of microstructure, texture and residual stresses in selective laser melted superalloy Inconel 718. *Mater Des*. 2017;134:139-150.

    doi: 10.1016/j.matdes.2017.08.049

47. Mazumder J. Laser direct metal deposition technology and microstructure and composition segregation of Inconel 718 superalloy. *J Iron Steel Res Int*. 2011;18(4):73-78.

    doi: 10.1016/S1006-706X(11)60054-X

48. Wang F, Ma D, Buhrig-Polaczek A. Microsegregation behavior of alloying elements in single-crystal nickel-based superalloys with emphasis on dendritic structure. *Mater Charact*. 2017;127:311-316.

    doi: 10.1016/j.matchar.2017.02.030

49. Shi Z, Dong J, Zhang M, Zheng L. Solidification characteristics and segregation behavior of Ni-based superalloy K418 for auto turbocharger turbine. *J Alloys Compd*. 2013;571:168-177.

    doi: 10.1016/j.jallcom.2013.03.241

50. Feng S, Zhang N, Luo X. Influence of segregation on liquid density in the mushy zone of DZ483 Ni-based superalloy. *Acta Metall Sin*. 2012;48(5):541-546.

    doi: 10.3724/SP.J.1037.2012.00037

51. Liang YJ, Cheng X, Wang HM. A new microsegregation model for rapid solidification multicomponent alloys and its application to single-crystal nickel-base superalloys of laser rapid directional solidification. *Acta Mater*. 2016;118:17-27.

    doi: 10.1016/j.actamat.2016.07.008

52. Ojo OA, Chaturvedi MC. On the role of liquated γ′ precipitates in weld heat affected zone microfissuring of a nickel-based superalloy. *Mater Sci Eng A*. 2005;403(1-2):77-86.

    doi: 10.1016/j.msea.2005.04.034

53. Sidhu RK, Ojo OA, Chaturvedi MC. Microstructural response of directionally solidified Rene' 80 superalloy to gas-tungsten arc welding. *Metall Mater Trans A*. 2009;40(1):150-162.

    doi: 10.1007/s11661-008-9700-5

54. Rush MT, Colegrove PA, Zhang Z, Broad D. Liquation and post-weld heat treatment cracking in Rene 80 laser repair welds. *J Mater Process Technol*. 2012;212(1):188-197.

    doi: 10.1016/j.jmatprotec.2011.09.001

55. Chen Y, Lu FG, Zhang K, *et al.* Laser powder deposition of carbon nanotube reinforced nickel-based superalloy Inconel 718. *Carbon*. 2016;107:361-370.

    doi: 10.1016/j.carbon.2016.06.014

56. Harrison NJ, Todd I, Mumtaz K. Reduction of micro-cracking in nickel superalloys processed by selective laser melting: A fundamental alloy design approach. *Acta Mater*. 2015;94:59-68.

    doi: 10.1016/j.actamat.2015.04.035

57. Zhong M, Sun H, Liu W, Li J, Zhu X, He J. Boundary liquation and interface cracking characterization in laser deposition of Inconel 738 on directionally solidified Ni-based superalloy. *Scr Mater*. 2005;53(2):159-164.

    doi: 10.1016/j.scriptamat.2005.03.047

58. Zhao XM, Lin X, Chen J, Xue L, Huang WD. The effect of hot isostatic pressing on crack healing, microstructure, and mechanical properties of Rene88DT superalloy prepared by laser solid forming. *Mater Sci Eng A*. 2009;504:29-134.

    doi: 10.1016/j.msea.2008.12.024

59. Nematzadeh F, Akbarpour MR, Parvizi S, Kokabi AH, Sadrnezhaad SK. Effect of welding parameters on microstructure, mechanical properties and hot cracking phenomenon in Udimet 520 superalloy. *Mater Des*. 2012;36:94-99.

    doi: 10.1016/j.matdes.2011.10.020

60. Idowu OA, Ojo OA, Chaturvedi MC. Effect of heat input on heat affected zone cracking in laser welded ATI Allvac 718Plus superalloy. *Mater Sci Eng A*. 2007;454:389-397.

    doi:10.1016/j.msea.2006.11.054

61. Bian HY, Zhai XY, Wang SJ, Li Y, Wang W. Influence of heat input and thermal cycling on the crack and microstructure of laser deposition repair DZ125 alloy. *Rare Met Mater Eng*. 2020;49:1701-1706.

    doi: 10.12442/j.issn.1002-185X.20190156

62. Ebrahimnia M, Ghaini FM, Shahverdi HR. Hot cracking in pulsed laser processing of a nickel-based superalloy built up by electrospark deposition. *Sci Technol Weld Join*. 2014;19(1):25-29.

    doi: 10.1179/1362171813Y.0000000157

63. Chen ZJ, Zhang QL, Lou CH, Yao JH. Methods of crack control for inconel 738 laser cladding layer. *Appl Laser*. 2013;33(1):7-13.

64. Han Q, Gu Y, Setchi R, *et al*. Additive manufacturing of high-strength crack-free Ni-based Hastelloy X superalloy. *Addit Manuf*. 2019;30:100919.

    doi: 10.1016/j.addma.2019.100919

65. Hu YL, Lin X, Zhang SY, *et al*. Effect of solution heat treatment on the microstructure and mechanical properties of Inconel 625 superalloy fabricated by laser solid forming. *J Alloys Comp*. 2018;767:330-344.

    doi: 10.1016/j.jallcom.2018.07.087

66. Hu YL, Lin X, Lu XF, *et al*. Evolution of solidification microstructure and dynamic recrystallisation of Inconel 625 during laser solid forming process. *J Mater Sci*. 2018;53:15650-15666.

    doi: 10.1007/s10853-018-2701-x

67. Li X, Shi JJ, Wang CH, *et al*. Effect of heat treatment on microstructure evolution of Inconel 718 alloy fabricated by selective laser melting. *J Alloys Compd*. 2018;764:639-649.

    doi: 10.1016/j.jallcom.2018.06.112

68. Chlebus E, Gruber K, Kuźnicka B, Kwaśny W, Sałacinski T. Effect of heat treatment on the microstructure and mechanical properties of Inconel 718 processed by selective laser melting. *Mater Sci Eng A*. 2015;639:647-655.

    doi: 10.1016/j.msea.2015.05.035

69. Zhang H, Li C, Liu Y, *et al*. Effect of hot deformation on γ″ and δ phase precipitation of Inconel 718 alloy during deformation and isothermal treatment. *J Alloys Compd*. 2017;716:65-72.

    doi: 10.1016/j.jallcom.2017.05.042

70. Konečná R, Nicoletto G, Kunz L, Bača A. Microstructure and directional fatigue behavior of Inconel 718 produced by selective laser melting. *Procedia Struct Integr*. 2016;2: 2381-2388.

    doi: 10.1016/j.prostr.2016.06.298

71. Zhang F, Ilavsky J, Lindwall G, Stoudt M, Levine L, Allen A. Solid-state transformation of an additively manufactured Inconel 625 alloy at 700°C. *Appl Sci*. 2021;11:8643.

    doi: 10.3390/app11188643

72. Lass EA, Stoudt MR, Katz MB, Williams ME, Ghosh G, Levine LE. Precipitation and dissolution of δ and γ″ during heat treatment of a laser powder-bed fusion produced Ni-based superalloy. *Scr Mater.* 2018;154:83-86.

    doi: 10.1016/j.scriptamat.2018.05.025

73. Marchese G, Bassini E, Parizia S, *et al*. Role of the chemical homogenization on the microstructural and mechanical evolution of prolonged heat-treated laser powder bed fused Inconel 625. *Mater Sci Eng A*. 2020;796:140007.

    doi: 10.1016/j.msea.2020.140007

74. Lass EA, Stoudt MR, Williams ME, *et al*. Formation of the $Ni_3Nb$ δ-phase in stress-relieved Inconel 625 produced via laser powder-bed fusion additive manufacturing. *Metall Mater Trans A Phys Metall Mater Sci*. 2017;48(11): 5547-5558.

    doi: 10.1007/s11661-017-4304-6

75. Luna V, Trujillo L, Gamon A, *et al*. Comprehensive and comparative heat treatment of additively manufactured Inconel 625 alloy and corresponding microstructures and mechanical properties. *J Manuf Mater Process*. 2022;6:107.

    doi: 10.3390/jmmp6050107

76. Rosenthal S, Platt S, Hoelker-Jaeger R. Forming properties of additively manufactured monolithic Hastelloy X sheets. *Mater Sci Eng A*. 2019;753:300-316.

    doi: 10.1016/j.msea.2019.03.035

77. Zhang F, Levine LE, Allen AJ, *et al*. Effect of heat treatment on the microstructural evolution of a nickel-based superalloy additive manufactured by laser powder bed fusion. *Acta Mater*. 2018;152:200-214.

    doi: 10.1016/j.actamat.2018.03.017

78. Dinda GP, Dasgupta AK, Mazumder J. Texture control during laser deposition of nickel-based superalloy. *Scr Mater*. 2012;67(5):503-506.

    doi: 10.1016/j.scriptamat.2012.12.028

79. Ma D, Stoica AD, Wang Z, Beese AM. Crystallographic texture in an additively manufactured nickel-base superalloy. *Mater Sci Eng A*. 2017;684:47-53.

    doi: 10.1016/j.msea.2016.11.110

80. Sui S, Tan H, Chen J, *et al.* The influence of Laves phases on the room temperature tensile properties of Inconel 718 fabricated by powder feeding laser additive manufacturing. *Acta Mater*. 2019;164:413-427.

    doi: 10.1016/j.actamat.2018.10.032

81. Sui S, Chen J, Fan E, Yang H, Lin X, Huang W. The influence of Laves phases on the high-cycle fatigue behavior of laser additive manufactured Inconel 718. *Mater Sci Eng A*. 2017;695:6-13.

    doi: 10.1016/j.msea.2017.03.098

82. Wu S, Peng HZ, Gao X, *et al*. Improving creep property of additively manufactured Inconel 718 through specifically designed post heat treatments. *Mater Sci Eng A*. 2022;857:144047.

    doi: 10.1016/j.msea.2022.144047

83. Guo J. The effect of aluminum and titanium on the microstructure and mechanical properties of an iron-base alloy. *Acta Metall Sin*. 1978;14(3):227-234.

84. Li X, Chen B, Xing W, *et al*. Effect of Si on solidification behavior and mechanical property of superalloy K4169. *Chin J Mater Res*. 2018;32(12):936-945.

    doi: 10.11901/1005.3093.2018.181

85. Sullivan CP, Donachie MJ. Microstructures and mechanical properties of iron-base (containing) superalloys. *Met Eng Q*. 1971;4(11):1.

86. Ling L, Han Y, Zhou W, *et al.* Study of microsegregation and Laves phase in Inconel 718 superalloy regarding cooling rate during solidification. *Metall Mater Trans A*. 2015;46(1):1-8.

    doi: 10.1007/s11661-014-2614-5

87. Xiao H, Li S, Han X, Mazumder J, Song L. Laves phase control of Inconel 718 alloy using quasi-continuous-wave laser additive manufacturing. *Mater Des*. 2017;122:330-339.

    doi: 10.1016/j.matdes.2017.03.004

88. Xiao H, Li SM, Xiao WJ, *et al.* Effects of laser modes on Nb segregation and Laves phase formation during laser additive manufacturing of nickel-based superalloy. *Mater Lett*. 2017;188:260-262.

    doi: 10.1016/j.matlet.2016.10.118

89. Tucho WM, Cuvillier P, Sjølst-Kverneland A, Hansen V. Microstructure and hardness studies of Inconel 718 manufactured by selective laser melting before and after solution heat treatment. *Mater Sci Eng A*. 2017;689:220-232.

    doi: 10.1016/j.msea.2017.02.062

90. Dinda GP, Dasgupta AK, Mazumder J. Laser aided direct metal deposition of Inconel 625 superalloy: Microstructural evolution and thermal stability. *Mater Sci Eng A*. 2009;509(1):98-104.

    doi: 10.1016/j.msea.2009.01.009

91. Kreitcberg A, Brailovski V, Turenne S. Effect of heat treatment and hot isostatic pressing on the microstructure and mechanical properties of Inconel 625 alloy processed by laser powder bed fusion. *Mater Sci Eng A*. 2017;689:1-10.

    doi: 10.1016/j.msea.2017.02.038

92. Thomas A, El-Wahabi M, Cabrera JM, Prado JM. High temperature deformation of Inconel 718. *J Mater Process Technol*. 2006;177(1-3):469-472.

    doi: 10.1016/j.jmatprotec.2006.04.072

93. Liu F, Lin X, Song M, *et al*. Effect of intermediate heat treatment temperature on microstructure and notch sensitivity of laser solid-formed Inconel 718 superalloy. *J Wuhan Univ Technol Mater Sci Ed*. 2011;26(5):908-913.

    doi: 10.1007/s11595-011-0335-9

94. Azadian S, Wei L, Warren R. Delta phase precipitation in Inconel 718. *Mater Charact*. 2004;53(1):7-16.

    doi: 10.1016/j.matchar.2004.07.004

95. Cai D, Zhang W, Nie P, Liu W, Yao M. Dissolution kinetics of δ phase and its influence on the notch sensitivity of Inconel 718. *Mater Charact*. 2007;58(3):220-225.

    doi: 10.1016/j.matchar.2006.04.020

96. Li S, Zhuang J, Yang J, *et al.* The effect of δ-phase on crack propagation under creep and fatigue conditions in Alloy 718. In: Loria EA, editor. *Superalloys 718, 625, 706 and Various Derivatives*. Warrendale, PA: TMS; 1994. p. 545-556.

97. Sundararaman M. Evolution of δ phase microstructure in Alloy 718. In: *Superalloy 718, 718+ and 907: Proceedings of the 7th International Symposium on Superalloy 718 and Derivatives*. United States: John Wiley & Sons; 2010. p. 139-152.

    doi: 10.1002/9781118762488.ch11

98. Ye N, Cheng M, Zhang S, Song HW, Zhou HW, Wang PB.

Effect of δ phase on mechanical properties of GH4169 alloy at room temperature. *J Iron Steel Res Int*. 2015;22(8):752-756.

doi: 10.1016/S1006-706X(15)30068-6

99. Yuan Z, Liu J, Zhang S. Research on precipitation kinetics of δ-phase in GH4169 alloy. *J Shenyang Ligong Univ*. 2010;29(2):23-26.

100. Deng G, Tu S, Zhang X, *et al.* Small fatigue crack initiation and growth mechanisms of nickel-based superalloy GH4169 at 650°C in air. *Eng Fract Mech*. 2016;153:35-49.

doi: 10.1016/j.engfracmech.2015.12.014

101. Hong B, Yi X, Meng QC. Effect of δ-$Ni_3Nb$ on low-cycle fatigue fracture of Inconel 718. *Acta Metall Sin*. 1994;27(2):79-82.

102. Zhang XC, Li HC, Zeng X, Tu ST, Zhang CC, Wang CQ. Fatigue behavior and bilinear Coffin-Manson plots of Ni-based GH4169 alloy with different volume fractions of δ phase. *Mater Sci Eng A*. 2017;682:12-22.

doi: 10.1016/j.msea.2016.11.040

103. Zhang H, Zhang S, Cheng M. Effect of δ phase on the tensile deformation behavior of GH4169 alloy at high temperature. *Acta Metall Sin*. 2013;29(4):483-488.

doi: 10.3724/SP.J.1037.2012.00620

104. Wang RYZ, Zhang XC, Liu F, Yao LL, Tu ST. Fatigue and fracture behaviors of nickel-based forging GH4169 superalloy and optimization of model parameters. *Procedia Eng*. 2015;130:1088-1096.

doi: 10.1016/j.proeng.2015.12.270

105. Zhang H, Li C, Guo Q, *et al*. Hot tensile behavior of cold-rolled Inconel 718 alloy at 650°C: the role of δ phase. *Mater Sci Eng A*. 2018;722:136-146.

doi: 10.1016/j.msea.2018.02.093

106. Ning Y, Huang S, Fu MW, Dong J. Microstructural characterization, formation mechanism, and fracture behavior of the needle δ phase in Fe–Ni–Cr-type superalloys with high Nb content. *Mater Charact*. 2015;109:36-42.

doi: 10.1016/j.matchar.2015.09.011

107. Cao GH, Sun TY, Wang CH, *et al*. Investigations of γ′, γ″, and δ precipitates in heat-treated Inconel 718 alloy fabricated by selective laser melting. *Mater Charact.* 2018;136:398-406.

doi: 10.1016/j.matchar.2018.01.015

108. Tiley J, Viswanathan GB, Hwang JY, Srinivasan R, Lipsitt HA. Evaluation of gamma prime volume fractions and lattice misfits in a nickel-base superalloy using the external standard X-ray diffraction method. *Mater Sci Eng A*. 2010;528(1):32-36.

doi: 10.1016/j.msea.2010.07.036

109. Drexler A, Oberwinkler B, Primig S, *et al*. Experimental and numerical investigations of the γ″ and γ′ precipitation kinetics in Alloy 718. *Mater Sci Eng A*. 2018;723:314-323.

doi: 10.1016/j.msea.2018.03.013

110. Collins DM, Stone HJ. A modelling approach to yield strength optimisation in a nickel-base superalloy. *Int J Plast*. 2014;54:96-112.

doi: 10.1016/j.ijplas.2013.08.009

111. Slama C, Abdellaoui M. Structural characterization of the aged Inconel 718. *J Alloys Compd*. 2000;306(1-2):277-284.

doi: 10.1016/S0925-8388(00)00789-1

112. Srinivas S, Prasad KS, Gopikrishna D, Venugopal P. Stress rupture in hot-rolled superalloy 718: Property-microstructure correlation. *Mater Charact*. 1995;35(2):93-98.

doi: 10.1016/1044-5803(95)80108-1

113. Ming X, Chen J, Tan H, *et al*. Coarsening behavior of γ″ precipitates in GH4169 superalloy fabricated by laser solid forming. *J Mater Eng*. 2014;8:8-14.

114. Chaturvedi MC, Han Y. Effect of particle size on the creep rate of superalloy Inconel 718. *Mater Sci Eng*. 1987;89:7-10.

doi: 10.1016/0025-5416(87)90264-3

115. Wan HY, Luo YW, Zhang B, *et al*. Effects of surface roughness and build thickness on fatigue properties of selective laser melted Inconel 718 at 650°C. *Int J Fatigue*. 2020;137:105654.

doi: 10.1016/j.ijfatigue.2020.105654

116. Ma XF, Zhai HL, Zuo L, *et al*. Fatigue short crack propagation behavior of selective laser melted Inconel 718 alloy by *in-situ* SEM study: Influence of orientation and temperature. *Int J Fatigue*. 2020;139:105739.

doi: 10.1016/j.ijfatigue.2020.105739

117. Yu X, Lin X, Wang Z, *et al*. Room and high temperature high-cycle fatigue properties of Inconel 718 superalloy prepared using laser directed energy deposition. *Mater Sci Eng A*. 2021;825:141865.

doi: 10.1016/j.msea.2021.141865

118. Zhang S, Weng K, Guo C, *et al*. The creep behavior of IN718 alloy fabricated by selective laser melting compared to forging. *Appl Mater Today*. 2024;38:102252.

doi: 10.1016/j.apmt.2024.102252

119. Shi Q, Zhang S, Dong X, Wang H, Liu Y, Zhang X. Achieving superior resistance to high-temperature creep in laser powder bed fusion of Inconel 718 via grain boundary serration. *J Mater Res Technol*. 2024;33:7534-7545.

doi: 10.1016/j.jmrt.2024.11.038

120. Spierings AB, Dawson K, Kern K, Stanojevic A, Weber R. SLM-processed Sc- and Zr-modified Al-Mg alloy: Mechanical properties and microstructural effects of heat treatment. *Mater Sci Eng A*. 2017;701:264-273.

doi: 10.1016/j.msea.2017.06.089

121. Sreeramagiri P, Bhagavatam A, Ramakrishnan A, Alrehaili H, Dinda GP. Design and development of a high-performance Ni-based superalloy WSU 150 for additive manufacturing. *J Mater Sci Technol*. 2020;47:20-28.

doi: 10.1016/j.jmst.2020.01.041

122. Tang YT, Panwisawas C, Ghoussoub JN, *et al.* Alloys-by-design: application to new superalloys for additive manufacturing. *Acta Mater*. 2021;202:417-436.

doi: 10.1016/j.actamat.2020.09.023

123. Kou S. A criterion for cracking during solidification. *Acta Mater*. 2015;88:366-374.

doi: 10.1016/j.actamat.2015.01.034

124. Song W, Yang J, Liang J, *et al.* A new approach to design advanced superalloys for additive manufacturing. *Addit Manuf*. 2024;84:104098.

doi: 10.1016/j.addma.2024.104098

125. Sun Z, Soh V, Lee C, Tan MJ, Bi G, Zhou W. Effects of carbon content on precipitate evolution and crack susceptibility in additively manufactured IN738LC. *Mater Sci Addit Manuf*. 2024;3(1):2264.

doi: 10.36922/msam.2264

126. Hong C, Gu DD, Dai DH, Zhang D, Wen M. Laser additive manufacturing of ultrafine TiC particle reinforced Inconel 625 based composite parts: Tailored microstructures and enhanced performance. *Mater Sci Eng A*. 2015;635:118-128.

doi: 10.1016/j.msea.2015.03.043

127. Gu DD, Hong C, Jia Q, Dai DH, Zhang D. Combined strengthening of multi-phase and graded interface in laser additive manufactured TiC/Inconel 718 composites. *J Phys D Appl Phys*. 2014;47(4):045309.

doi: 10.1088/0022-3727/47/4/045309

128. Gu DD, Zhang HM, Dai DH, Zhang D, Wen M. Laser additive manufacturing of nano-TiC reinforced Ni-based nanocomposites with tailored microstructure and performance. *Compos Part B Eng*. 2019;163:585-597.

doi: 10.1016/j.compositesb.2018.12.146

129. Cao SN, Gu DD. Laser metal deposition additive manufacturing of TiC/Inconel 625 nanocomposites: Relation of densification, microstructures, and performance. *J Mater Res*. 2015;30(23):3616-3628.

doi: 10.1557/jmr.2015.358

130. Zhang BC, Bi GJ, Sun CN, Dong ZL, Bi J. Microstructure and mechanical properties of Inconel 625/nano-$TiB_2$ composite fabricated by LAAM. *Mater Des*. 2016;111:70-79.

doi: 10.1016/j.matdes.2016.08.078

131. Yang W, He W, Hu Z, Zhang X, Liu Y, Wang H. Fabrication of Inconel 718 composites reinforced with TiCN via laser powder bed fusion: Integration of triply periodic minimal surface lattice structures. *J Mater Res Technol*. 2024;32:2443-2458.

doi: 10.1016/j.jmrt.2024.08.102

132. Gruber K, Stopyra W, Kobiela K, Kurzynowski T, Skiba M, Szczepański T. Achieving high strength and ductility in Inconel 718: Tailoring grain structure through micron-sized carbide additives in PBF-LB/M additive manufacturing. *Virtual Phys Prototyp*. 2024;19(1):e2396064.

doi: 10.1080/17452759.2024.2396064

133. Wang P, Zhang BC, Liu J, Du X. Microstructural characteristics and mechanical properties of carbon nanotube reinforced Inconel 625 parts fabricated by selective laser melting. *Mater Des*. 2016;112:290-299.

doi: 10.1016/j.matdes.2016.09.080

134. Deng PS, Yao CW, Feng K, *et al.* Enhanced wear resistance of laser cladded graphene nanoplatelets reinforced Inconel 625 superalloy composite coating. *Surf Coat Technol*. 2018;335:334-344.

doi: 10.1016/j.surfcoat.2017.12.047

135. Xiao WH, Lu SQ, Wang YC, *et al.* Mechanical and tribological behaviors of graphene/Inconel 718 composites. *Trans Nonferrous Met Soc China*. 2018;28:1958-1969.

doi: 10.1016/S1003-6326(18)64841-1